Article

Cell Reports

Rif1 Regulates the Fate of DNA Entanglements during Mitosis

Graphical Abstract

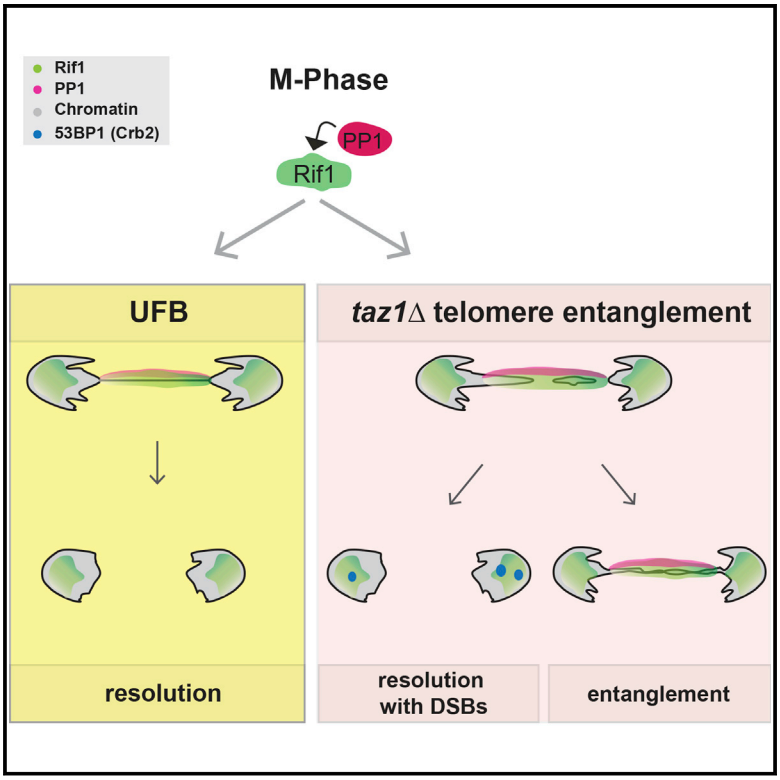

Authors

Sophie Zaaijer, Nadeem Shaikh, Rishi Kumar Nageshan, Julia Promisel Cooper

Correspondence

julie.cooper@nih.gov

In Brief

Zaaijer et al. show that the conserved DNA replication and repair protein Rif1 promotes resolution of non-telomeric DNA entanglements at anaphase, but further entwines entanglements between dysfunctional telomeres. This anaphase role is distinct from Rif1's activities in S phase and G2 but shares the requirement for Rif1 to interact with protein phosphatase 1.

Highlights

- Telomere replication problems lead to DNA entanglements persisting in anaphase
- Rif1 specifically acts in anaphase to inhibit entanglement resolution
- Anaphase Rif1 function promotes the resolution of non-telomeric entanglements

Zaaijer et al., 2016, Cell Reports *16*, 148–160
June 28, 2016
http://dx.doi.org/10.1016/j.celrep.2016.05.077

OPEN ACCESS
CellPress

Cell Reports
Article

Rif1 Regulates the Fate of DNA Entanglements during Mitosis

Sophie Zaaijer,[1,2] Nadeem Shaikh,[1] Rishi Kumar Nageshan,[1] and Julia Promisel Cooper[1,*]
[1]Laboratory of Biochemistry and Molecular Biology, Center for Cancer Research, National Cancer Institute, NIH, Bethesda, MD 20892, USA
[2]Present address: New York Genome Center, 101 Avenue of the Americas, New York, NY 10013, USA
*Correspondence: julie.cooper@nih.gov
http://dx.doi.org/10.1016/j.celrep.2016.05.077

SUMMARY

Clearance of entangled DNA from the anaphase mid-region must accurately proceed in order for chromosomes to segregate with high fidelity. Loss of Taz1 (fission yeast ortholog of human TRF1/TRF2) leads to stalled telomeric replication forks that trigger telomeric entanglements; the resolution of these entanglements fails at $\leq$20°C. Here, we investigate these entanglements and their promotion by the conserved replication/repair protein Rif1. Rif1 plays no role in *taz1Δ* fork stalling. Rather, Rif1 localizes to the anaphase mid-region and regulates the resolution of persisting DNA structures. This anaphase role for Rif1 is genetically separate from the role of Rif1 in S/G2, though both roles require binding to PP1 phosphatase, implying spatially and temporally distinct Rif1-regulated phosphatase substrates. Rif1 thus acts as a double-edged sword. Although it inhibits the resolution of *taz1Δ* telomere entanglements, it promotes the resolution of non-telomeric ultrafine anaphase bridges at $\leq$20°C. We suggest a unifying model for Rif1's seemingly diverse roles in chromosome segregation in eukaryotes.

INTRODUCTION

By the time a cell divides, all chromosomes need to be equally partitioned between the two separated chromatid masses; DNA persisting in the middle of an anaphase cell threatens the integrity of the inherited genome. Nonetheless, a growing number of studies have revealed the tenacious presence of DNA in the anaphase mid-region, implying a dramatic last-minute scramble by the cell to clear the region and ensure faithful genomic segregation. In particular, challenges during S phase can result in entwined sister DNA strands, catenated duplexes, or strand invasion intermediates. Failure to resolve any of these structures results in chromosome entanglements.

Chromosomal entanglements can manifest as fine DNA-containing strands persisting between segregating DNA masses, referred to as ultrafine anaphase bridges or UFBs (Baumann et al., 2007; Chan et al., 2007). UFBs are distinct from anaphase bridges comprising whole lagging chromosomes, which often originate from merotelic attachments in which single centromeres are attached and pulled simultaneously to both poles (reviewed in Gregan et al., 2011); in addition, whereas lagging chromosomes are clearly coated with histones, the latter have rarely been detected on UFBs (Chan and Hickson, 2011). Mammalian UFBs are generally visualized by immunofluorescence using antibodies against proteins implicated in UFB resolution. Most commonly, UFBs originate from centromeric DNA and may represent loops arising from defective replication of the repeated centromeric units or catenated centromeric duplex sister chromatids; such centromeric UFBs are seen in unperturbed cells in early anaphase and do not impact wild-type (WT) cell viability (Baumann et al., 2007; Chan et al., 2007). These UFBs are decorated by PICH (Plk1-interacting protein) (Baumann et al., 2007) and the BLM helicase, and their levels are increased on treatment with topoisomerase II inhibitors (Baumann et al., 2007; Chan et al., 2007). A second type of UFB, thought to originate from persisting late replication intermediates, is characterized by the additional presence of the FANCD2 and FANCI DNA repair proteins at sites flanking the UFBs, as well as RPA along the intervening stretch (Chan and Hickson, 2011; Chan et al., 2009). UFBs of this class are rare, but increase in frequency in cells treated with replication inhibitors. This type of UFB can generate a DNA double-strand break (DSB) response in the daughter nuclei during the ensuing G1 phase, as indicated by formation of 53BP1 foci (Chan et al., 2009; Lukas et al., 2011).

Although PICH constitutes a robust marker for mammalian UFBs (Baumann et al., 2007), no PICH ortholog has been identified in *Saccharomyces cerevisiae* or *Schizosaccharomyces pombe*. Nonetheless, UFB-like structures have been reported in *S. pombe* strains experiencing replication stalling at lacO/I arrays that serve as bidirectional barriers to replication fork progression (Sofueva et al., 2011); such arrays are clearly visible as UFBs. Formation and removal of these UFBs is Rad51 independent, as is also true for mammalian UFBs (Chan et al., 2009). In *S. cerevisiae*, UFBs also have been suggested to originate from induced fork barriers and are coated by RPA, $Dpb11^{TopBP1}$, and $Sgs1^{BLM}$ (Germann et al., 2014; Sofueva et al., 2011).

As highly repetitive genomic regions, telomeres are notorious for challenging replication (Barefield and Karlseder, 2012; Miller et al., 2006; Sfeir et al., 2009). The telomere binding protein Taz1 mitigates the tendency of telomere repeats to impede replication in *S. pombe* (Miller et al., 2006); this ability to promote telomere replication has been shown to be a conserved role

for the mammalian Taz1 ortholog, TRF1 (Sfeir et al., 2009). Stalled RFs in *taz1Δ* cells are aberrantly processed upon sumoylation and activation of the RecQ helicase Rqh1 (a BLM ortholog), rendering them unable to restart (Rog et al., 2009). These irreversibly stalled forks lead to a number of phenotypes, including sub-telomeric hyper-recombination, immediate telomere loss on telomerase inactivation, and cold-sensitive viability. Hence, at temperatures of ≤20°C, *taz1Δ* cells show associations between the separating chromatin masses that fail to resolve at mitosis; we refer to these *taz1Δ* DNA bridges as telomere entanglements. These entanglements are distinct from telomere fusions, as the absence of Lig4, the ligase required for non-homologous end joining (NHEJ), fails to rescue their occurrence (Miller and Cooper, 2003); moreover, they are not products of Rad51-dependent homologous recombination, as *taz1Δ* cold sensitivity is not rescued by Rad51 inhibition. The origin of telomere entanglements in stalled RFs is further illustrated by comparing cells lacking Taz1 versus cells lacking Rap1, a Taz1-binding protein. While *taz1Δ* and *rap1Δ* strains share several phenotypes (including elongated telomeres, loss of telomere position effect, and susceptibility to NHEJ-mediated fusions during G1 arrest), *rap1Δ* telomeres do not suffer replication fork stalling and therefore do not experience entanglement or reduced viability in colder environments (Miller et al., 2005, 2006). A phenomenon reminiscent of *taz1Δ* telomere entanglements, in which NHEJ-independent telomere associations are seen between mitotic chromosomes, has been observed in mammalian TRF1-deficient cells experiencing compromised telomere replication (Muñoz et al., 2009; Ohishi et al., 2014; Sfeir et al., 2009). Moreover, stalled telomeric RFs provoked by the depletion of the ReqQ helicase WRN, or aphidicolin treatment, generate UFBs (Barefield and Karlseder, 2012). Hence, telomere disentanglement represents a universal challenge to genome stability.

Rif1 is a highly conserved and multifaceted protein, first identified as a budding yeast telomere length regulator (Hardy et al., 1992). ScRif1 associates with telomeres via Rap1 binding (Hardy et al., 1992; Shi et al., 2013); it also appears to bind the single-strand (ss) overhangs or ss/ds junctions at telomeres (Xu et al., 2010), where it plays a role in limiting 5′ telomeric resection and preventing cell-cycle arrest (Xue et al., 2011). Although mammalian Rif1 has not been implicated in telomere length regulation, it controls the choice of DNA repair pathway at internal DSBs and dysfunctional telomeres, favoring NHEJ by inhibiting resection of 5′ ends (Chapman et al., 2013; Di Virgilio et al., 2013; Escribano-Díaz et al., 2013; Silverman et al., 2004; Xu and Blackburn, 2004; Zimmermann et al., 2013). Moreover, both yeast and mammalian Rif1 play key roles in replication initiation, as well as in the replication timing program; in the absence of Rif1, many late-firing origins fire early and vice versa (Cornacchia et al., 2012; Hayano et al., 2012; Lian et al., 2011; Yamazaki et al., 2013). The roles of yeast Rif1 in replication have been linked to interaction of protein phosphatase 1 (PP1) with the SILK/RvXF motif in the N-terminal region of Rif1 (Davé et al., 2014; Mattarocci et al., 2014). The presence of PP1 at *S. pombe* origins opposes phosphorylation of the replicative MCM helicases by the Dbf4-dependent kinase (DDK). Phosphorylation of Rif1 in S phase promotes the release of PP1, allowing DDK-mediated phosphorylation to trigger origin firing (Davé et al., 2014). Finally, consistent with an additional function for Rif1 beyond the foregoing S- and interphase-based functions, mammalian Rif1 has been observed in the mid-region between separating chromatin masses at anaphase (Hengeveld et al., 2015; Xu and Blackburn, 2004).

Remarkably, deletion of *rif1+* suppresses the cold sensitivity of *taz1Δ* cells, implicating Rif1 as a causative factor in telomere entanglements (Miller et al., 2005). Fission yeast Rif1 was heretofore thought to bind telomeres in a Taz1-dependent manner (Kanoh and Ishikawa, 2001), further deepening the mystery of its role in a *taz1Δ* setting. Here, we address the basis for these observations. We show that when telomeric replication fork progression is challenged, DNA entanglements persist into anaphase, a period in which intense processing activities are observed. We find that Rif1 acts neither to promote telomeric fork stalling nor to prevent fork restart. Rather, it acts via a previously unrecognized role to inhibit the resolution of *taz1Δ* telomeres during anaphase. Conversely, the timely segregation of centromeric UFBs is promoted by Rif1. Hence, Rif1 acts as a double-edged sword, increasing the efficiency of resolution of WT UFBs while inhibiting resolution of entangled *taz1Δ* telomeres. We further show that PP1 binding by Rif1 is required for Rif1's dual roles in facilitating chromosome segregation in the presence of Taz1, while confounding chromosome segregation in the absence of Taz1. Collectively, our data suggest Rif1 as a key universal regulator of the final steps of chromatid segregation.

RESULTS

Telomere Entanglements Persist in Anaphase, when Inefficient Resolution Engenders Problems in the Next Cell Cycle

Stalled RFs at *taz1Δ* telomeres are processed into telomere entanglements (Miller and Cooper, 2003; Miller et al., 2005, 2006), the resolution of which fails at cold temperatures (≤20°C) (Miller and Cooper, 2003). To explore the nature of these entanglements in greater detail, we used live-cell microscopy to analyze *taz1Δ* cells harboring RFP-tagged histones at 32°C and 19°C. Patterns of chromosome segregation were categorized as wild-type like (WT-like) or aberrant. During WT-like chromosome segregation, sister chromatids equally segregate as compact entities to opposite poles (Figure 1A; Movies S1, S2, and S3). The aberrant category comprises two patterns: one dubbed the "pointing finger," in which unresolved connections persist between segregating chromosome masses, evinced by protrusions of condensed histone-rich regions. These connections appear to resolve in late anaphase, as they abruptly retract toward the main chromatin masses. The second sub-category, "irreversibly entangled," refers to cases in which chromatin persists between the main chromosome masses and fails to resolve.

At the normal growing temperature (32°C), 15% of *taz1Δ* cells show the pointing finger pattern, but no reduction of viability (Figure 1B). After shifting cultures from 32°C to 19°C, the proportion of cells displaying aberrant segregation patterns increases and continues to increase progressively with longer incubation at cold temperature (Figure 1B) This progressive increase with

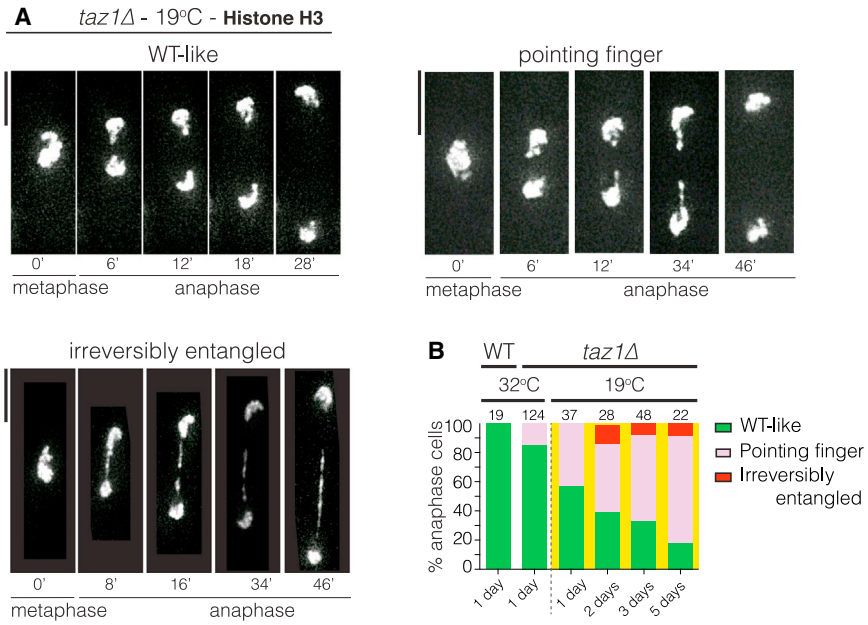

Figure 1. Telomere Entanglements Fail to Resolve in the Cold

(A) Film stills showing examples of chromosome segregation patterns through mitosis. Chromatin is visualized using Hht1-mRFP (histone H3 tagged at one of the two *hht1*$^{+}$ loci). Scale bars in this and all subsequent microscopy images represent 5 μm.

(B) Quantitation of morphologies depicted in (A). Cells grown at 32°C were shifted to 19°C for the stated number of days (x axis labels) and maintained in log phase throughout. Numbers above bars indicate n-values.

See also Movies S1, S2, and S3.

successive cell divisions suggests a cumulative accrual of defects due to inapt resolution of telomere entanglements.

taz1Δ Entanglements Occur via Telomeres, Rather than via rDNA, and Are Mainly between Sister Chromatids

In WT anaphase, we consistently observe four Taz1 foci lagging behind the other eight Taz1 foci that colocalize with the main chromatin masses (Figure 2A). As *S. pombe* has three chromosomes (and therefore 12 telomeres per nucleus at anaphase onset), we wondered whether the four persisting foci represent sister telomeres of one specific chromosome; in particular, the rDNA repeat regions reside at either end of chr3 (Figure 2B). The rDNA binding factor Reb1 was used to visualize the rDNA (Figure 2B) given that visible histone H3 localization is excluded from the rDNA regions. Reb1-coated chromosome arms remain in the mid-region after the bulk of chromatin has segregated, implying that the four Taz1 foci persisting between chromatin masses in WT anaphase represent the telomeres at either end of chr3 (compare Figure 2A to Figure 2B).

Given that the rDNA-adjacent telomeres tend to segregate last in a WT setting, do the DNA strands persisting between aberrantly segregating chromatin masses in a *taz1Δ* setting represent rDNA? Whereas rDNA segregates last in ~70% of WT cells at both 32°C and 19°C, this percentage drops to ~30% in *taz1Δ* cells, in which protruding histone-rich regions comprise the majority of persisting mid-region chromatin (Figures 2C and 2D). Hence, the unsegregated regions in *taz1Δ* anaphase are not confined to the rDNA, but rather comprise the ends of all three chromosomes.

To determine whether *taz1Δ* entanglements occur between telomeres of sister or non-sister chromatids, we utilized a strain harboring a LacO/LacI-GFP array at the *sod2* locus ("*sod2-lacO/I-GFP*") ~80 kb from the left telomere of chr1 (Ding et al., 2004). In *taz1Δ* cells exhibiting WT-like chromosome segregation, the *sod2-lacO/I-GFP* foci are always clearly embedded in both of the main chromatin masses at anaphase (Figure 2E, top right). Of those cells demonstrating aberrant chromosome segregation, two GFP foci remain in the mid-region in 40% of cases (Figure 2E), indicating one or more entanglement(s) involving both sisters of chr1. However, in 14% of missegregants, only one *sod2-lacO/I-GFP* focus persists in the mid-region, whereas the other focus has segregated, indicating an entanglement between telomere IL and a non-sister chromatid. In the remaining ~40% of defective segregants, both *sod2-lacO/I-GFP* foci clearly lie within the segregated masses and not within the intervening stretch, suggesting entanglements that did not involve chr1. Hence, stalled *taz1Δ* RFs preferentially lead to entanglements between sister telomeres, but strand invasion can occur between any combination of telomeres and occasionally link non-sisters. Conceivably, only non-sister entanglements lead to cold sensitivity.

Telomere Entanglements Remain Connected by ssDNA

The existence of unresolved DNA intermediates in the anaphase mid-region of *taz1Δ* cells prompted us to investigate which proteins co-localize with, and perhaps regulate the resolution of, these DNA stretches. Endogenous tagging of the shelterin component Tpz1, which associates with ss-telomeric overhangs as well as the ds telomere binding proteins, revealed Tpz1 foci between segregating DNA masses (Figure S1A). These foci tend to be interspersed with histone H3 foci in a non-overlapping pattern, suggesting that the intervening DNA comprises interspersed ss and ds regions.

The ssDNA binding complex RPA binds and stabilizes unwound DNA during replication and repair and serves as a platform for repair factors. We investigated RPA localization using an endogenously tagged allele of its Rad11 subunit. Unperturbed WT cells show the expected pattern of RPA localization, with foci appearing only during S phase (Figure 3A). In contrast, *taz1Δ* cells show one or two pronounced Rad11^{RPA} foci throughout the cell cycle (Carneiro et al., 2010). Intriguingly, the DNA stretching between anaphase *taz1Δ* chromatin masses is abundantly coated with Rad11^{RPA} at both 32°C and 19°C (Figures 3B and 3C); the stretch can be flanked by one or two particularly large and intense RPA foci, likely representing clumps of

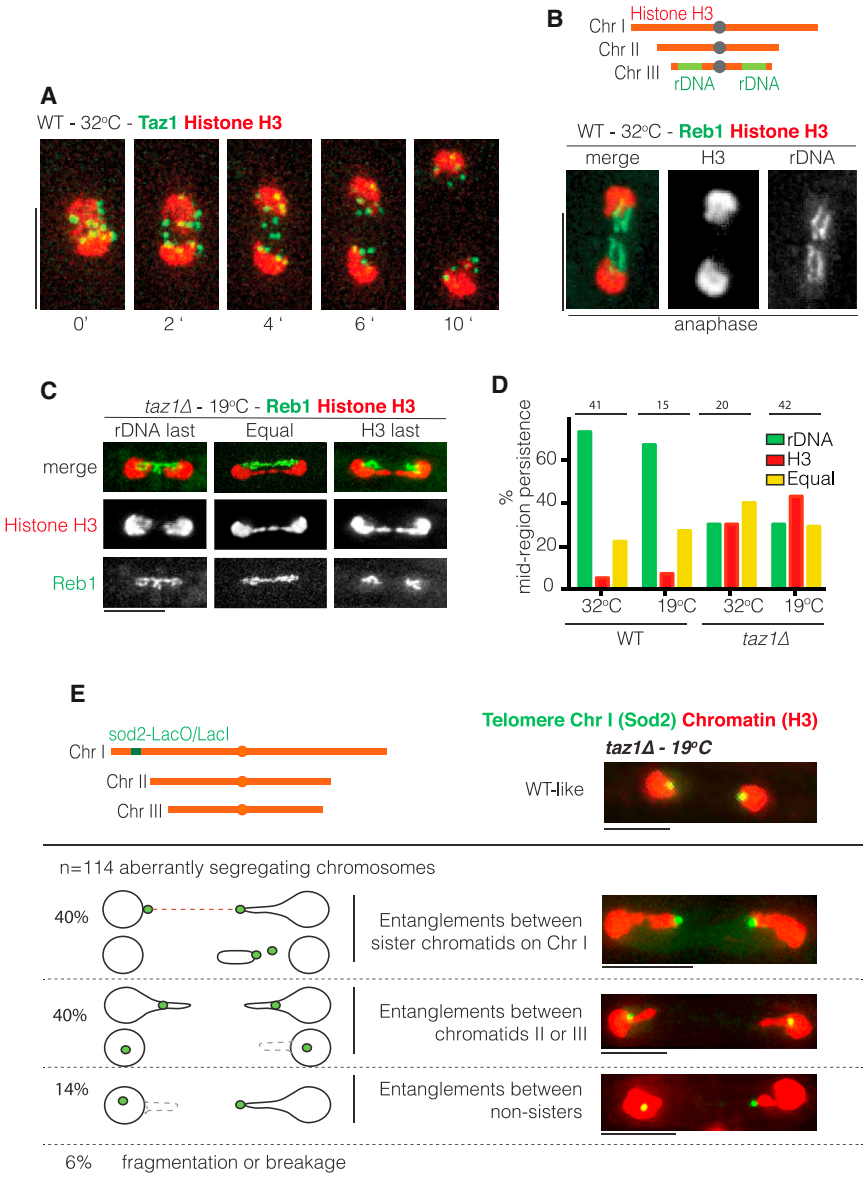

Figure 2. *taz1Δ* Telomere Entanglements Occur between Both Sister and Non-sister Chromatids and Do Not Involve rDNA

(A) Film stills of a typical WT cell. Telomeres are visualized with Taz1-GFP (endogenously tagged) and chromatin as in Figure 1. Numbers indicate time since metaphase onset.

(B) Above: schematic of *S. pombe* genome indicating the positions of rDNA on chromosome 3 (chr3). Below: rDNA is viewed via endogenously tagged Reb1 (a transcriptional termination factor specific for rDNA) and chromatin as in Figure 1. In WT anaphase, the rDNA-containing ends of chr3 segregate last (quantified in D).

(C) As in (B). Left: in the absence of *taz1*$^{+}$, a subset of cells shows a WT segregation pattern (rDNA last). Middle: example of *taz1Δ* cell in which non-rDNA and rDNA chromosome ends segregate simultaneously (equal). Right: *taz1Δ* cell in which the rDNA segregates earlier than other chromosome ends (H3 last).

(D) Quantitation of (C). Cells were grown to log phase at 32°C and then scored after overnight growth at 19°C.

(E) Top left: schematic indicating the position of *sod2-lacO/I-GFP* near telomere 1L. Below: phenotypes of *taz1Δ* cells observed *via sod2-lacO/I-GFP* are indicated. Top right: no entanglements. Chart below: types of aberrant segregation patterns. Top: telomere entanglements involve both chr1 sister chromatids. Panels below: cells with entanglements that do not involve chr1 or involve telomere IL and a different chromosome arm (i.e., between non-sisters). Fragmentation or breakage refers to cells showing multiple *sod2-lacO/I-GFP* foci or, rarely, both foci at the same pole.

entangled ssDNA. Structured illumination microscopy (SIM) reveals that ss-stretches can originate from multiple sites within the same cell, evinced by forked structures (Figures 3C and 3D). Moreover, time-lapse microscopy reveals that the RPA-coated stretches are dynamic, retracting over the course of anaphase (Figure 3E). While the presence of Rad11^{RPA} stretches is observed in *taz1Δ* cells at both 32°C and 19°C, their frequency in fields of still images of anaphase *taz1Δ* cells increases when temperature is reduced (from 26% at 32°C to 54% at 19°C).

Intrigued by the persistence of ssDNA stretches, we investigated other DNA replication and repair factors that play roles in ssDNA degradation or fill-in. DNA polymerase α (Pol α, encoded by fission yeast *swi7+*) is a lagging strand DNA polymerase with roles in genome-wide replication and synthesis of the strand complementary to the telomere repeats added by telomerase. In WT cells, Pol α appears in foci only during S phase (Figure S1B). By contrast, Pol α remains associated with telomere entanglements in G2 in *taz1Δ* cells at 32°C and 19°C. Moreover, these foci persist in anaphase on *taz1Δ* telomere entanglements at 19°C (Figure S1B).

Rad52, a homologous recombination factor recruited downstream of RPA to promote strand invasion, is required for viability of *taz1Δ* cells in the cold (Miller and Cooper, 2003). Likewise, Rad52 localizes to the anaphase mid-region in a pattern similar to that of RPA^{Rad11} (Figure S1C).

Checkpoint Arrest Is Provoked in Response to Inappropriate Resolution of Telomere Entanglements

When *taz1Δ* cells are grown at 32°C, their telomeres co-localize with components of the DNA damage response pathway, yet they avoid cell-cycle arrest (Carneiro et al., 2010). This avoidance was shown to stem from local histone modification state; methylation of histone H4 lysine 20 is required for binding by the checkpoint mediator Crb2^{53BP1}, but H4-K20 methylation is excluded from telomeric chromatin (Carneiro et al., 2010). In contrast, *taz1Δ* cells do activate the checkpoint at 19°C, as indicated by Rad3^{ATR}/Chk1-dependent cell elongation (Miller and Cooper,

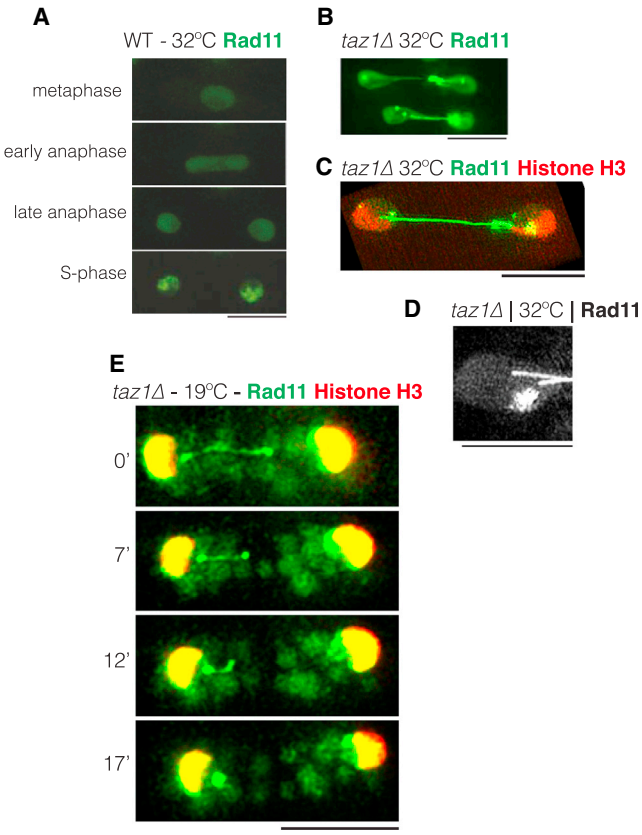

Figure 3. RPA Decorates the Strands Persisting between Anaphase *taz1Δ* Chromatin Masses

(A) Representative images of cells with endogenously tagged Rad11^{RPA}, viewed as in Figure 1. In WT cells, Rad11^{RPA} foci are detectable as foci only during S phase.

(B) *taz1Δ* cells viewed as in (A). In anaphase, Rad11^{RPA} stretches from one chromatin mass to the other.

(C) Structural illumination microscopy (SIM) images of *taz1Δ* cells with Rad11^{RPA} tagged as in (A) and histone H3 as in Figure 1.

(D) Magnified and rotated image of the left pole of the cell shown in (C). The forked structure suggests the simultaneous presence of two entanglements.

(E) Film frames of anaphase with tags as in (C). Rad11^{RPA} retracts progressively. See also Figure S1 and Movie S4.

2003). The accrual of *taz1Δ* chromosomal defects over time at 19°C suggests an explanation for this. Whereas stalled *taz1Δ* RFs, which occur at 32°C as well as at 19°C, fail to trigger checkpoint activation, damage arising from transmission of inappropriately resolved telomere entanglements into the next cell cycle may trigger checkpoint activation. To evaluate this possibility, we monitored several hallmarks of cell-cycle progression and/or arrest. Both WT and *taz1Δ* cells respond within 1 hr of cold treatment by accumulating transiently in the mono-nucleate state, indicating a brief metaphase arrest. In WT cultures, binucleate cells, representing progression through mitosis, start to arise at 3 hr; soon thereafter, RPA appears in such binucleates, indicating S phase initiation (note that fission yeast begins S phase before septation is complete; Figures S2A and S2B). In *taz1Δ* cultures, this timing is altered. *taz1Δ* cell length increases gradually (Figure S2C). Initiation of anaphase following cold induction is delayed compared to WT (Figures S2A and S2B), indicating a brief metaphase arrest, as reported previously (Miller and Cooper, 2003). Consistent with the idea that G2/M DNA damage checkpoint instigation follows progression to the following cell cycle, Crb2^{53BP1} foci start to appear in *taz1Δ* cells 3 hr after the temperature shift and increase in number thereafter (Figure S2D). Moreover, *taz1Δ* cell elongation at $\leq$20°C requires Crb2^{53BP1} (Figure S2E). Hence, Crb2^{53BP1} foci fail to form in the first S/G2 phase following temperature shift. Instead, they form later, in response to damage incurred during M phase and carried into subsequent cell cycles.

Rif1 Is Specifically Involved in Telomere Entanglement

Rif1 has been implicated as causative of telomere entanglements through the observation that *rif1+* deletion rescues *taz1Δ* cold sensitivity (Miller et al., 2005). Rif1's involvement could stem from a role in initiating fork stalling events, in processing stalled forks, or in downstream processes that promote the formation—or inhibit the resolution—of entanglements (Germe et al., 2009; Rog et al., 2009). To tease apart these possibilities, we addressed each stage of the genesis of entanglements. We analyzed telomere replication intermediates using 2D gel electrophoresis. As previously reported, *taz1Δ* telomeres generate a distinct "plume" pattern reflecting the inability of forks to reach the end of the elongated *taz1Δ* telomeres (Miller et al., 2006) (Figure S3A). This *taz1Δ* plume pattern is unaffected by *rif1+* deletion. Moreover, the fork stalling seen at an internally inserted telomere repeat stretch in a *taz1Δ* setting is unaffected by *rif1+* deletion (Figure S3B). Therefore, Rif1's role in telomere entanglement does not reflect a role in the initial genesis of stalled RFs.

The inability to fully replicate *taz1Δ* telomeres renders their maintenance fully dependent on telomerase; hence, in the absence of the telomerase catalytic subunit (Trt1), telomeres are rapidly lost despite their initial over-elongation (Miller et al., 2006). Consistent with the observation that Rif1's presence has no impact on fork stalling, *trt1+* deletion in a *taz1Δrif1Δ* background yields the same rapid loss of telomeres as seen in the *taz1Δ* background (Figure 4A). This result also rules out a role for Rif1 in converting stalled RFs to irreversibly stalled RFs and contrasts with the role of Rqh1 in that conversion (Rog et al., 2009). Accordingly, *rif1+* deletion fails to rescue *taz1Δ* sub-telomeric hyper-recombination or the propensity of *taz1Δ* telomeres to survive telomerase loss via hyper-recombination (Figure 4B), both outcomes of stalled *taz1Δ* RFs. We conclude that Rif1 specifically acts in the generation or resolution of telomere entanglements downstream of irreversibly stalled *taz1Δ* RFs.

To explore Rif1's role downstream of the stalled RFs, we analyzed chromosome segregation dynamics. A clear reduction in chromosome segregation defects is observed when comparing *taz1Δrif1Δ* and *taz1Δ* cells grown in the cold (compare Figure 1B with Figure 4C). However, the occurrence of Rad11^{RPA} -bound stretches between sister chromatids during anaphase is not affected by the loss of Rif1 (Figure 4D). These observations suggest that Rif1 is involved not in forming entanglements, but rather in inhibiting their proper resolution.

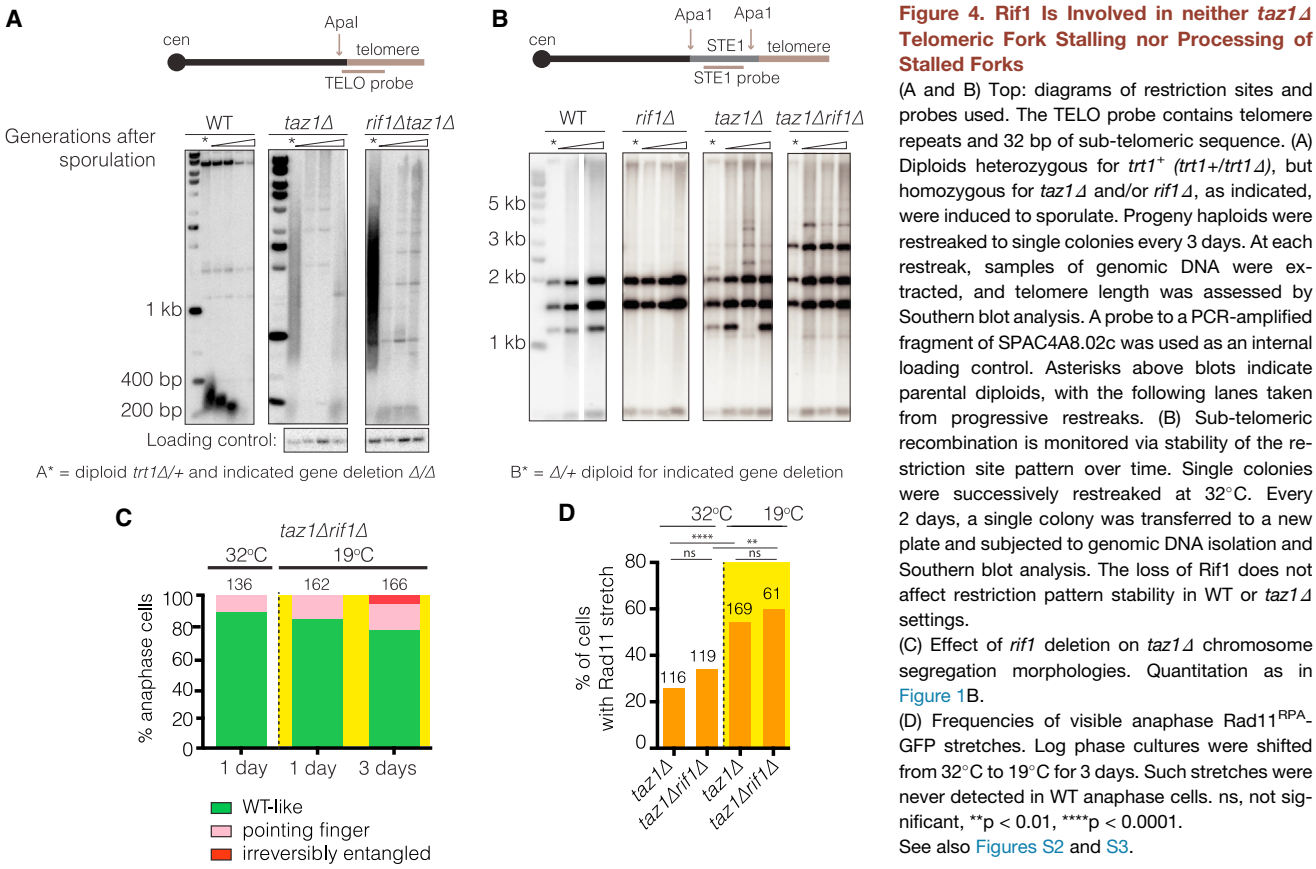

Figure 4. Rif1 Is Involved in neither *taz1Δ* Telomeric Fork Stalling nor Processing of Stalled Forks

(A and B) Top: diagrams of restriction sites and probes used. The TELO probe contains telomere repeats and 32 bp of sub-telomeric sequence. (A) Diploids heterozygous for *trt1*$^{+}$ *(trt1+/trt1Δ)*, but homozygous for *taz1Δ* and/or *rif1Δ*, as indicated, were induced to sporulate. Progeny haploids were restreaked to single colonies every 3 days. At each restreak, samples of genomic DNA were extracted, and telomere length was assessed by Southern blot analysis. A probe to a PCR-amplified fragment of SPAC4A8.02c was used as an internal loading control. Asterisks above blots indicate parental diploids, with the following lanes taken from progressive restreaks. (B) Sub-telomeric recombination is monitored via stability of the restriction site pattern over time. Single colonies were successively restreaked at 32°C. Every 2 days, a single colony was transferred to a new plate and subjected to genomic DNA isolation and Southern blot analysis. The loss of Rif1 does not affect restriction pattern stability in WT or *taz1Δ* settings.

(C) Effect of *rif1* deletion on *taz1Δ* chromosome segregation morphologies. Quantitation as in Figure 1B.

(D) Frequencies of visible anaphase Rad11^{RPA}-GFP stretches. Log phase cultures were shifted from 32°C to 19°C for 3 days. Such stretches were never detected in WT anaphase cells. ns, not significant, $^{**}p < 0.01$, $^{****}p < 0.0001$.

See also Figures S2 and S3.

Mammalian Rif1 has been implicated in the DNA damage response as a 53BP1-dependent inhibitor of 5′ end resection (Chapman et al., 2013; Di Virgilio et al., 2013; Escribano-Díaz et al., 2013; Zimmermann et al., 2013). The observations that fission yeast *rif1+* deletion yields neither DNA damage sensitivity (Davé et al., 2014; Hayano et al., 2012) nor altered levels of 5′ resection in WT or *taz1Δ* settings (Miller et al., 2005) weigh against the notion that SpRif1 generates *taz1Δ* cold sensitivity by inhibiting 5′ resection. Moreover, it is unlikely that SpRif1 is involved in channeling repair to NHEJ as is mammalian Rif1 (Chapman et al., 2013; Di Virgilio et al., 2013; Zimmermann et al., 2013; Escribano-Díaz et al., 2013), since *rif1+* deletion has no impact on the NHEJ-dependent telomere fusions seen in G1 arrested *taz1Δ* cells (Miller et al., 2005). To explore this further, we investigated the role of the fission yeast 53BP1 ortholog, Crb2, in *taz1Δ* telomere entanglement. *crb2+* deletion fails to suppress *taz1Δ* cold sensitivity (Figure S2F), again indicating that Rif1 acts independently of Crb2 to exacerbate *taz1Δ* entanglements.

Rif1 Is Present in the Anaphase Mid-region

If Rif1 inhibits the resolution of telomere entanglements at anaphase, then we might expect it to localize to the anaphase mid-region. To investigate this possibility, we turned to live microscopy. C-terminally GFP-tagged Rif1 acts as a *rif1* null, rescuing both *taz1Δ* cold sensitivity and the lethality of the DDK mutant *hsk1-89* (Figures S4A and S4B). Moreover, whereas C-terminally Myc-GFP-tagged Rif1 is functional, expression levels yield insufficient fluorophore signal for detailed analysis. We therefore placed N-terminally tagged Rif1 under control of the inducible *nmt41* promoter. Growth of *nmt41-GFP-rif1* cells under partially repressed conditions allows visualization of GFP-Rif1 without affecting viability in either WT or *taz1Δ* backgrounds (Figure S4C). GFP-Rif1 appears as a nuclear haze with distinct foci co-localizing with Taz1, as previously shown (Kanoh and Ishikawa, 2001) (Figure S4D). Surprisingly, Rif1 shows two distinct categories of localization in WT mitotic cells. First, Rif1 localizes to segregating Taz1 foci, which appears at all telomeres (Figure S4E). Second, Rif1 forms a stretch of foci between segregated anaphase chromatin masses (Figure 5A). Higher resolution live imaging suggests two Rif1 "sliding arms" in the mid-region; these arms shorten on spindle elongation (Figure 5C).

Rif1's localization to the anaphase mid-region appears at a time and place not occupied by Taz1 (compare Figure 5A with Figure 2A). Accordingly, this category of Rif1 foci is seen in both *taz1+* and *taz1Δ* cells. However, these Rif1 foci are more often visible between aberrantly segregating than properly segregating chromosomes in *taz1Δ* cells (Figure 5B). Enhanced visibility reflects either longer duration or higher frequency of Rif1 mid-region localization in mis-segregants, consistent with a role in inhibiting resolution of entanglements.

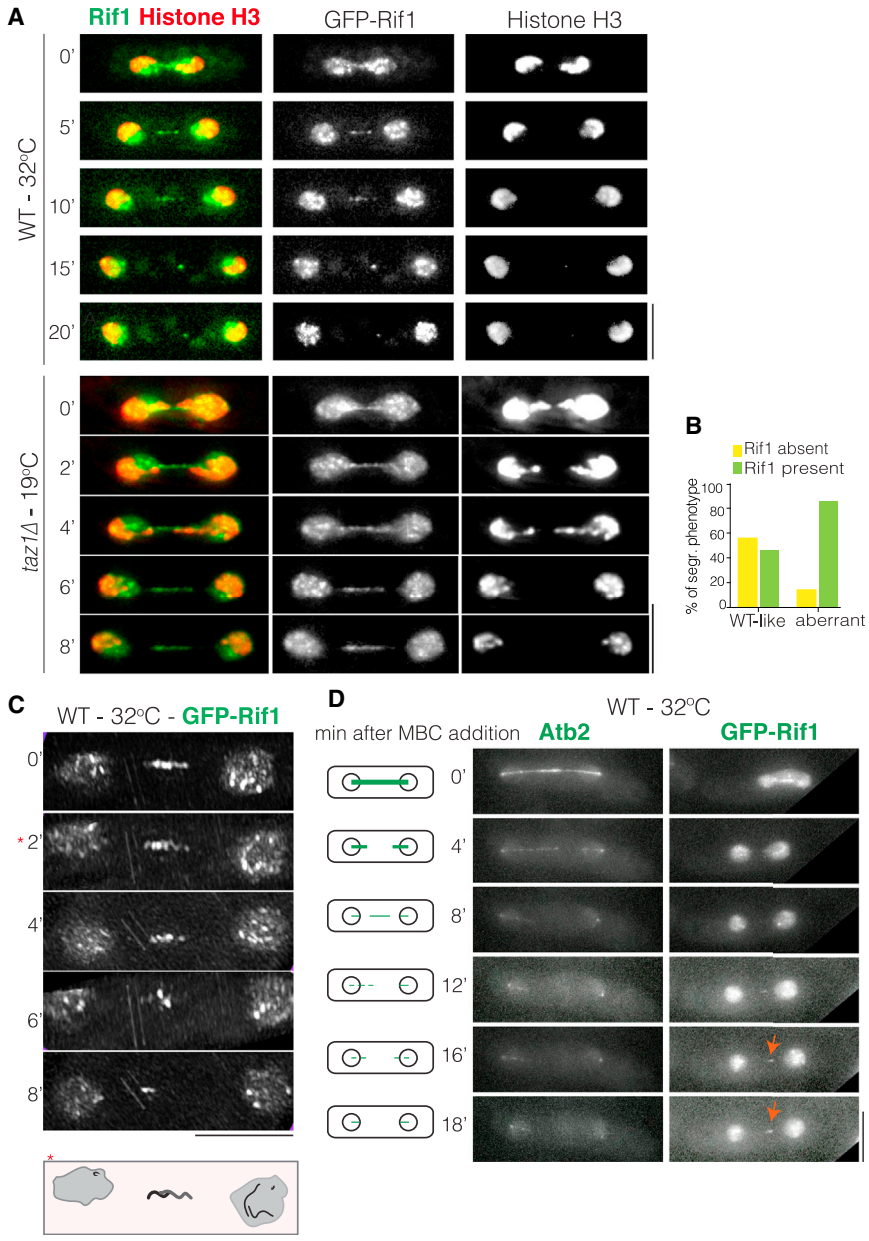

Figure 5. Rif Localizes to Anaphase Mid-region

(A) Frames from films of WT cells at 32°C or *taz1Δ* cells grown to log phase at 32°C and then shifted to 19°C for 24 hr. Rif1 is N-terminally GFP-tagged under *nmt41* promoter control and histone H3 tagged as in Figure 1. GFP-Rif1 lingers in the mid-region as cells complete anaphase. Compare with Figure S4E.

(B) Quantitation of GFP-Rif1 stretches during WT-like or aberrant chromosome segregation in *taz1Δ* cells.

(C) SIM of GFP-Rif1 in anaphase. For each panel, the image is rotated to the orientation that yields the clearest signal. The pattern suggests interlocking helical strands (diagram below).

(D) Cells with either an extra copy of the gene encoding α-tubulin (*atb2+*, under *nmt1* control) or Rif1 tagged as in (A) were grown at 32°C and mixed in one microscope dish. Anaphase, as detected via the presence of a mitotic spindle or two segregating nuclei harboring GFP-Rif1, was filmed. At time point 0', MBC was added and cells were imaged every 2 min to follow MBC-induced spindle depolymerization. Dissipation of the Atb2 signal (i.e., the spindle) is clearly seen; nonetheless, GFP-Rif1 in adjacent cells (subject to identical MBC treatment in the same dish) clearly persists in the mid-region (red arrow).

See also Figure S4.

How is Rif1 recruited to the anaphase mid-region? A previous study suggested that human Rif1 binds anaphase microtubules (Xu and Blackburn, 2004), whereas a more recent study localized Rif1 to UFBs (Hengeveld et al., 2015). To determine whether spindle microtubules are required for Rif1 localization, we assessed whether spindle depolymerization would affect Rif1 localization. While treatment of live cells with methyl 2-benzimidazole carbamate (MBC) efficiently depolymerizes spindle microtubules (Figure 5D), Rif1 foci remain unaltered by MBC treatment, indicating spindle-independent localization. Moreover, overexposure of the histone H3 signal reveals a thin stretch between anaphase chromatids, either co-localizing with or adjacent to Rif1 (Figure S4F).

Rif1 Promotes Timely Resolution of Centromere-Proximal UFBs

Are our observations that Rif1 inhibits resolution of *taz1Δ* telomeric entanglements relevant to other types of entangled structures? To expand our analysis beyond telomeric DNA, we turned to a non-telomeric region. A Tomato-tagged Tet repressor (TetR) bound to a repetitive *tetO* array integrated within the centromere of chr2 ("*cenII-tetO/R-Tomato*") blocks efficient RF progression and appears in UFBs (Sofueva et al., 2011). *cenII-tetO/R-Tomato* forms a single bright focus in each G2 cell, whereas unbound TetI generates a general nuclear haze in cells lacking the *tetO* array (Figure 6A). In WT cells at 32°C, the *tetO/R-Tomato* focus separates at metaphase to two foci that segregate neatly to opposite poles during anaphase. Intriguingly, however, in cultures grown at 19°C for 3 days, 8% of WT cells exhibit a *tetO/R-Tomato* stretch between the separating chromatid masses. Remarkably, *rif1+* deletion greatly exacerbated the occurrence of these UFBs, most pronouncedly at 19°C (Figures 6B and 6C). Hence, like UFBs comprising telomeric entanglements, non-telomeric UFBs arise more frequently and/or persist longer at cold temperature. However, in direct opposition to its role in telomeric entanglements, Rif1 plays a key cold-specific role in limiting the appearance of *tetO/R*-containing UFBs.

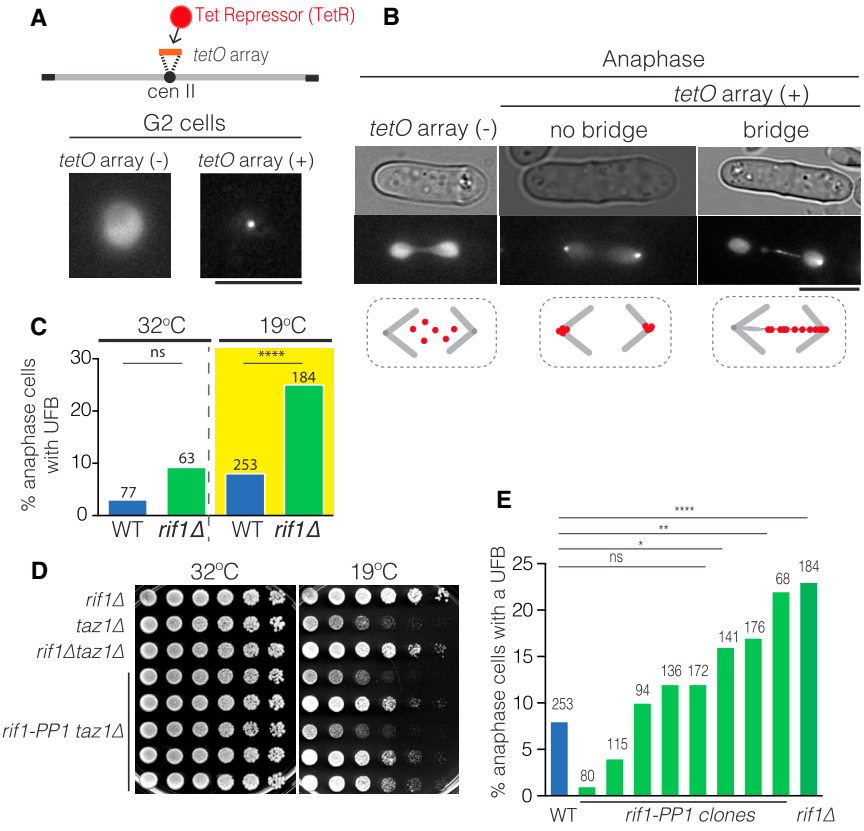

Figure 6. Rif1 Promotes Efficient UFB Resolution in WT Cells at ≤20°C and Requires PP1 Interaction

(A) Schematic indicates the location of the *tetO* array bound by TetR-tomato. Below: G2 cells expressing TetR-tomato with or without *cenII-tetO* array.

(B) Differential interference contrast (top) and fluorescence (bottom) images of TetR-tomato in anaphase cells without (–) or with (+) *cenII-tetO*. Interpretive diagrams are shown below.

(C) Quantitation of UFB frequencies. Cells with *cenII-tetO/R-tomato* were grown to log phase at 32°C and then shifted to 19°C for 3 days. ****$p < 0.0001$.

(D) 5-fold serial dilutions of log phase cells (32°C) were stamped and incubated at 32°C (2 days) or 19°C (5 days). *rif1-PP1* generates variable suppression of *taz1Δ* cold sensitivity.

(E) Quantitation of *cenII-tetO/R-tomato*-UFBs at 19°C. ns, not significant, *$p < 0.05$, ****$p < 0.0001$. See also Figure S5.

Phosphatase Binding by Rif1 Is Required for Rif1's Anaphase Activity

The SILK/RvXF motif at the N-terminal domain of Rif1 has been identified as the PP1 binding site (Sreesankar et al., 2012). Hence, while telomeres normally replicate late in S phase, the Rif1-PP1 mutant allele, which compromises PP1 binding, confers early telomere replication (Mattarocci et al., 2014; Davé et al., 2014; Hiraga et al., 2014). To determine whether phosphatase regulation mediates Rif1's roles in telomere length regulation or anaphase resolution of mid-region DNA structures, we assessed the effects of *rif1-PP1* on these parameters. Most cells harboring Rif1-PP1 show telomere elongation reminiscent of that conferred by *rif1Δ* (Figure S5A, left). This telomere elongation phenotype is incompletely penetrant with independent *rif1-PP1* isolates showing variable telomere length (Figure S5A, right), suggesting that the extent of PP1 exclusion varies between clones. Nonetheless, the clear occurrence of *rif1Δ* telomere length in *rif1-PP1* cells indicates that telomere length regulation by Rif1 is mediated, at least in part, by PP1 control. Consistently, cells harboring the Rif1-7A allele, which confers constitutive binding of PP1 to Rif1, show WT telomere length (Figure S5A).

To address the role of Rif1-associated PP1 in telomeric entanglement, we asked whether *rif1-PP1* rescues *taz1Δ* cold sensitivity as does *rif1Δ*. As was the case for telomere length regulation, clonal variation was observed, with approximately half of the *rif1-PP1* clones rescuing *taz1Δ* cold sensitivity (Figure 6D). This phenotypic mosaicism varies over successive generations; on restreaking for single colonies, a *rif1-PP1* clone that rescues cold sensitivity can give rise to clones that fail to rescue and vice versa (data not shown). Such reversibility indicates that the mosaicism is an inherent property of the *rif1-PP1* mutations rather than the emergence of suppressor mutations. Furthermore, deletion of the gene encoding the Dis2 PP1 rescues *taz1Δ* cold sensitivity to an extent comparable with *rif1Δ* and *rif1-PP1* (Figure S5B).

If Rif1's role in inhibiting the resolution of telomere entanglements stems from the same activity that confers Rif1's role in stimulating non-telomeric UFB resolution, then Rif1-PP1 should phenocopy *rif1Δ* in exacerbating the presence of UFBs. Remarkably, introduction of *rif1-PP1* into strains harboring *cenII-tetO/R-Tomato* generates a clonally variable increase in visible anaphase bridge formation (Figure 6E). Collectively, we conclude that Rif1-mediated recruitment of phosphatase activity to UFBs and telomere entanglements dictates the success of their resolution.

The Activities of Rif1 in S Phase Are Separable from Rif1's Anaphase Role in Regulating UFB Resolution

Our observations that *rif1+* deletion has no impact on *taz1Δ* telomeric fork progression, hyper-recombination, or immediate telomere loss on *trt1+* deletion, along with the co-localization of Rif1 with DNA stretches in the anaphase mid-region, strongly suggest that Rif1 acts at anaphase to regulate entanglement resolution and that this activity is not a by-product of Rif1's roles in controlling S-phase DNA transactions (e.g., replication origin firing or DSB resection). To further explore this idea, we sought to construct a Rif1 allele that would separate S- and M-phase functions. To achieve this, we placed Rif1 under control of the S-phase-specific promoter of *cdt1+*; the *cdt1+* promoter, along with a selectable marker at its 5′ end, was inserted directly upstream of endogenous *rif1+* (see Figure 7A for details). While WT *rif1+* is expressed to similar levels during S- or M-phase arrest, cells carrying *pcdt1-rif1* yield higher *rif1+* expression levels than WT cells

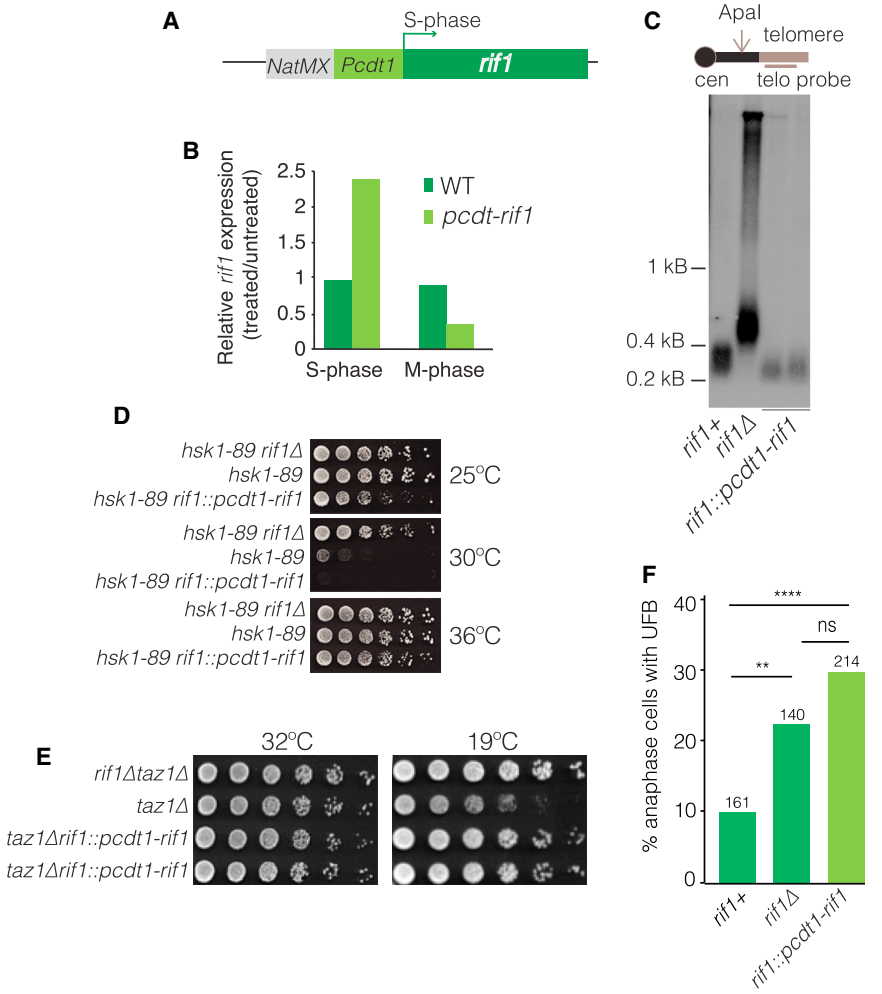

Figure 7. Rif1's Anaphase and S-Phase Functions Are Separate

(A) Schematic of approach to induce S-phase-specific *rif1+* expression. The *cdt1*$^+$ promoter region (640 bp, including the binding site for the S-phase transcription factor Cdc10 and *cdt1* transcription start site and 5′ UTR) was inserted immediately upstream of the endogenous *rif1* ORF. NatMx provides a selectable marker.

(B) Relative *rif1* transcript levels were determined by qRT-PCR and normalized to levels of *act1*. (S phase) Cells were grown in media containing 15 mM hydroxyurea (Sigma) for 4 hr at 32°C. (M phase) Cells were treated with 50 μg/ml TBZ (thiabendazole, a microtubule-depolymerizing agent) for 2 hr at 25°C. Arrest was verified via septation index.

(C) *pcdt1-rif1* confers WT telomere length, confirming S-phase function. Southern blot as in Figure 4. Two individual clones of the *pcdt1-rif1* strain were analyzed.

(D) *pcdt1-rif1* confers WT Rif1 function with respect to Hsk1-mediated replication control. 5-fold serial dilutions of log phase cells at 25°C (permissive for *hsk1-89*) incubated at 25°C, 30°C, or 36°C. While *rif1Δ* restores growth of *hsk1-89* cells at a non-permissive (30°C) temperature, *pcdt1-rif1* behaves as *rif1*$^+$ in failing to do so, confirming Rif1 functionality in S phase. Replicates grown at 36°C serve as loading control.

(E) Dilution assay as in (D). *pcdt1-rif1* behaves as *rif1Δ* by rescuing *taz1Δ* cold sensitivity.

(F) Frequencies of *cenII-tetO/R-tomato*-UFBs are quantified as in Figure 6C. *pcdt1-rif1* phenocopies *rif1Δ* in elevating UFB levels, tying UFB resolution to Rif1 function outside of S phase. **p < 0.01, ****p < 0.0001.

during S-phase arrest and lower levels than WT during an M-phase arrest (Figure 7B).

Functional expression of Rif1 during S/G2 was further tested by analyzing telomere length. Telomeres show WT length in *pcdt1-rif1* cells, indicating WT Rif1 function in S/G2 (Figure 7C). Moreover, *pcdt1-rif1* fails to phenocopy *rif1Δ* in rescuing the DDK mutant *hsk1-89*, again indicating WT Rif1 activity during S phase (Figure 7D). Strikingly, however, *pcdt1-rif1* fully mimics the *rif1+* null for rescue of *taz1Δ* cold sensitivity (Figure 7E). Moreover, *pcdt1-rif1* fully mimics the opposing effect of *rif1+* null in exacerbating the presence of non-telomeric UFBs harboring *cenII-tetO/R-Tomato* (Figure 7F) These data demonstrate that Rif1's activity at anaphase is indeed separable from its S-phase activities and that its anaphase activity is specifically responsible both for inhibiting resolution of telomere entanglements and stimulating resolution of non-telomeric UFBs.

DISCUSSION

This work sheds light on the complexity of resolving different types of DNA entanglements during anaphase, a period in which active repair and DNA synthesis processes remain underway, as evinced by the appearance of RPA, DNA polymerase α, and associated factors on telomeric entanglements in the anaphase mid-region. We have found a key role for Rif1 in regulating the cell's final attempt to separate persisting associations between segregating chromosomes. Remarkably, Rif1 can either help or hinder, depending on context. Rif1 helps this process by promoting timely resolution of the "WT" UFBs represented by *cenII-tetO/R* and hinders by inhibiting the resolution, and perhaps further interweaving, telomeric entanglements formed in *taz1Δ* cells. A unifying model for these seemingly paradoxical activities of Rif1 is presented below.

Rif1 in the *taz1Δ* Context

Loss of *taz1+* results in a host of dysfunctional telomere phenotypes, but *taz1Δ* cells are surprisingly viable, unless they are grown at cold temperatures (Miller and Cooper, 2003). Genetic and physical analyses have demonstrated that *taz1Δ* telomere entanglements originate from stalled RFs processed by Rqh1 to form DNA structures refractory to resumption of fork progression (Rog et al., 2009). Although resection at stalled *taz1Δ* RFs may play a role in entanglement (O. Rog and J.P.C., unpublished data), resection alone does not generate entanglements, as

rap1Δ telomeres suffer excessive resection with little entanglement (Miller et al., 2005). It is more likely that aberrant strand invasion events generate these entanglements.

Our microscopy-based analysis has uncovered a variety of proteins associated with the DNA stretches that span the segregating chromatin masses. Alternating patterns suggest that the DNA stretches comprise ssDNA regions (devoid of nucleosomes but coated with RPA) interspersed with dsDNA-wrapped nucleosomes. The RPA patterns are dynamic, with RPA-coated filaments retracting into one of the daughter cells during anaphase. We speculate that such retraction represents resolution of entanglement.

The observation that *taz1Δ* cells lose viability progressively over time in the cold suggests that resolution can be imperfect, leading to aberrant structures in the next cell cycle. Indeed, *taz1Δ* cells grown at cold temperatures accumulate high levels of DSBs (Miller and Cooper, 2003), likely a readout of inappropriate resolution or breakage of entangled chromosomes upon cell division. Consistently, $Crb2^{53BP1}$ foci only begin to appear after 3-hr growth of *taz1Δ* cells at 19°C; hence, Crb2 is recruited to DSBs, the genesis of which follows failed telomere entanglement resolution. This phenomenon resembles the progressive DSB accumulation reported to originate from UFBs generated by late replication intermediates; these UFBs trigger DSBs in daughter nuclei in the ensuing G1 phase (Chan et al., 2009).

The basis for the cold specificity of failed entanglement resolution is not yet known. Possibilities include the enhanced propensity for partially unwound DNA structures to reanneal in suboptimal conformations in the cold or a cold-sensitive activity of some DNA processing protein that limits entanglement. Whatever the basis for cold specificity, it serves as a useful property in linking roles of Rif1 that are specific to ≤20°C. These roles include not only the inhibition of *taz1Δ* entanglement resolution but also promotion of the robust resolution of non-telomeric UFBs. Indeed, the shared cold specificity of Rif1's involvement in *taz1Δ* entanglements and *cenII-tetO/R* UFBs provides compelling evidence for a common etiology.

Rif1: A Double-Edged Sword

While UFBs have been loosely defined as thin DNA strands not detectable by conventional DNA dyes, the term is applied to essentially distinct structures (see Introduction). Hence, the recognition of particular UFB types, and/or the processes that channel each type into an appropriate resolution pathway, may be prone to inaccuracy. Here, we have found that Rif1 may be responsible for such inaccuracy when UFBs harbor entangled telomeres. A plausible scenario is that Rif1 promotes the same anaphase activity at non-telomeric UFBs, entangled sister telomeres, and entangled non-sister telomeres; while this activity is beneficial for resolution of sister telomere entanglements, it is deleterious for non-sister telomeric entanglements. Indeed, while telomere entanglements mainly occur between sister chromatids, they connect non-sisters sufficiently frequently to account for the loss of viability we have observed at ≤20°C. One highly speculative but concrete idea for the basis for such opposing activities involves topoisomerase II (Top2). Given our previous work implicating Top2 in the resolution of telomere entanglements (Germe et al., 2009), Rif1 may promote Top2 activity in the specific orientation that removes entanglements between segments along a single chromosome. However, Top2 activity in this specific orientation could be envisioned to further entwine those telomeric entanglements that involve inter-chromosomal interactions.

Where Does Rif1 Bind?

The dynamic localization pattern of Rif1 places it precisely where resolution-promoting factors act during anaphase. We find that Rif1 localizes to the anaphase mid-region in a Taz1-independent fashion and lingers long after the bulk chromatin masses have segregated, coating thin stretches whose co-localization with histones is detectable only in single z stack microscopic sections. The first precedent for such Rif1 localization was reported in human cells, in which it was suggested to coincide with microtubules (Xu and Blackburn, 2004). Very recently, human Rif1 was reported to localize to UFBs in a microtubule-independent manner (Hengeveld et al., 2015). Likewise, our data show microtubule independent localization of Rif1 to the anaphase mid-region. Rif1 chromatin immunoprecipitation (ChIP)-chip assays have demonstrated both Taz1-dependent and Taz1-independent Rif1 binding sites, as well as differences in binding site profiles through the cell cycle (Hayano et al., 2012). Intriguingly, many of the Taz1-independent Rif1 binding sites correspond to sequences with the propensity to form G-quartet structures and indeed, a binding preference for the G-quartet configuration was demonstrated. It is conceivable that such secondary structures might form in the ss telomeric DNA regions intervening between anaphase chromosome masses, and might contribute to Rif1 recruitment. However, as the Rif1-regulated UFBs measured in the *cenII-tetO/R* assay lack G-quartet potential, the anaphase Rif1 recruitment mode cannot be primarily through G-quartet binding. We hypothesize that Rif1's recruitment to anaphase DNA structures occurs via non-sequence specific binding to ss/ds junctions, as Rif1 shows a binding preference for such regions (Xu et al., 2010), and entangled telomeres and non-telomeric UFBs are both replete with such ss/ds junctions.

Independent Roles for Rif1 in S Phase and Anaphase

A plethora of circumstantial evidence, along with construction of a key separation-of-function *rif1* allele, indicates that the function of Rif1 at anaphase is separable from its S/G2 phase functions. While Rif1 regulates origin firing and replication timing (Kanoh et al., 2015; Yamazaki et al., 2013), both *taz1Δ* and *taz1Δ rif1Δ* cells exhibit deregulated telomere replication timing (Dehé et al., 2012; Hayano et al., 2012), ruling out the possibility that altered replication timing underlies the effect of Rif1 on *taz1Δ* telomere entanglements. Moreover, Rif1 is clearly uninvolved in replication fork stalling at *taz1Δ* telomeres, sub-telomeric hyper-recombination, and the immediate telomere loss upon *trt1+* deletion seen in *taz1Δ* cells. These observations, along with the clear Taz1-independent localization of Rif1 to the anaphase mid-region, most parsimoniously place Rif1 as a regulator of entanglement resolution at anaphase.

The crucial clincher in our conception of Rif1 having separable roles in S/G2 and anaphase comes from the *cdt1-rif1* allele, which places Rif1 expression under the control of an S-phase-specific promoter. This allele retains the essentiality of DDK

kinase activity and confers WT telomere length, indicating robust Rif1 expression during S/G2. Nonetheless, *cdt1-rif1* clearly phenocopies the null in rescuing the cold sensitivity of *taz1Δ* cells and exacerbating the appearance of non-telomeric UFBs in the cold. Hence, S/G2 expression of Rif1 is irrelevant for entanglement resolution. Not only do these results separate S/G2 and anaphase Rif1 functions, but also they further highlight the connection between Rif1's opposing roles in resolving *taz1Δ versus cenII-tetO/R* UFBs, as both are products of Rif1 activity outside of S/G2.

Collectively, three hot-off-the-press reports reinforce the relevance of this study to our understanding human chromosome segregation and cancer. First, overexpression of hTRF2 leads to stalled telomeric RFs (Nera et al., 2015) reminiscent of those seen in *taz1Δ* fission yeast. Accordingly, telomere-containing UFBs are seen on hTRF2 overexpression, as are chromosome fusions presumably resulting from botched attempts of repair damage carried over from defective anaphases; this suite of phenotypes closely resembles those seen in *taz1Δ* cells grown in the cold. Given that hTRF2 is often overexpressed in cancer cells, such entanglement-mediated chromosome fusions are likely causative agents in tumorigenesis. The recent demonstration that hRIF1 localizes to UFBs further highlights the parallels with our system, suggesting that the anaphase role of fission yeast Rif1 is likely to be conserved. Finally, anaphase bridges resulting from dominant-negative inhibition of human TRF2 were shown to trigger chromothripsis when nuclear membrane rupture allows the cytoplasmic nuclease TREX1 to access the bridging DNA (Maciejowski et al., 2015). While the NHEJ-mediated telomere bridges induced by TRF2 inhibition are distinct from the entanglements studied here, the downstream DSBs in ensuing cell cycles could lead to NHEJ. This distinction highlights the need to understand the full range and regulation of anaphase chromosome separation pathways along with their downstream consequences.

Rif1 as a PP1 Platform Differently Utilized through Time and Space

While the full list of players and mechanistic details of Rif1 action at anaphase remain open questions, these anaphase activities share a dependence on PP1 binding with Rif1's role in coordinating the timing and initiation of DNA replication. The *rif1-PP1* allele shows variable penetrance with respect to telomere length, attenuation of *taz1Δ* cold sensitivity, and exacerbation of *cenII-tetO/R*-mediated UFBs alike. This variable penetrance may stem from the existence of two PP1 proteins in fission yeast, Sds21 and Dis2; while the *rif1-PP1* mutation vastly reduces the recruitment of Sds21 to telomeres, it may be more permissive to residual recruitment of Dis2 (Davé et al., 2014). This exchangeable interaction of the two PP1s could result in stochastically variable phosphatase activity.

The PP1 linkage suggests a unifying model for the apparently pleiotropic roles of Rif1. Binding to chromatin, whether via interactions with Taz1, G-quadruplex structures, ss/dsDNA junctions, or as-yet-undefined means, recruits PP1 activity to the relevant place and time. Once there, Rif1 will oppose local phosphorylation of PP1 substrates, creating the seemingly diverse set of chromatin-related functions attributed to Rif1. At replication origins, localized dephosphorylation will inhibit MCM-mediated origin firing; at sites of DNA damage, desphosphorylation may inhibit local resection activities; and at replicating telomeres, dephosphorylation clearly inhibits the extent of telomerase-mediated telomere extension. Likewise, dephosphorylation of kinase substrates localizing to the anaphase mid-region is likely to regulate resolution activities and may also control the rate of spindle elongation (data not shown). A candidate mid-region kinase ripe for opposition by Rif1-associated PP1 is Aurora B, a key component of the chromosomal passenger complex that relocates from kinetochores to the anaphase mid-region. Hence, Rif1 may be an adaptable chromatin-phosphatase interface, exploited to provide a brake on diverse phospho-proteins that act on partially unwound DNA.

EXPERIMENTAL PROCEDURES

Construction of S-rif1

To generate the *rif1::pcdt1-rif1* strain, four fragments (one comprising the 200-bp sequence immediately upstream of *rif1+*, one a 1.2-kb *natMX6* cassette [Sato et al., 2005], one comprising 640 bp of the *cdt1+* promoter sequence [Hofmann and Beach, 1994], and one comprising the first 200 bp of the *rif1+* ORF) were PCR amplified. The four fragments were then assembled into the pUC19 cloning vector using the Gibson Assembly Kit using the manufacturer's protocol (NEB). Correct orientation of all four fragments was confirmed by sequencing. The resultant *natMX6-pcdt1-rif1* construct was PCR amplified and transformed into WT cells; successful integration was confirmed by PCR. The *pcdt1-rif1 taz1Δ* strain was made in two ways: first, by crossing the *pcdt1-rif1* strain with a *taz1Δ* strain (Figure 7E) and, second, by transforming the *pcdt1-rif1* construct into *taz1Δ* cells as, well as into a heterozygous diploid (*rif1+/pcdt-rif1 taz1+/Δ*). Regardless of which of these strategies were used, all *pcdt1-rif1 taz1Δ* strains showed rescue of *taz1Δ* cold sensitivity.

SUPPLEMENTAL INFORMATION

Supplemental Information includes Supplemental Experimental Procedures, five figures, one table, and four movies and can be found with this article online at http://dx.doi.org/10.1016/j.celrep.2016.05.077.

AUTHOR CONTRIBUTIONS

S.Z. and J.P.C. designed and interpreted this study with contributions from N.S. and R.K.N. S.Z. performed the experiments in Figures 1–5 and S1–S5 with help from N.S. N.S. performed the work on non-telomeric UFBs, with help from S.Z. and R.K.N. R.K.N. performed the experiments on S-Rif1. S.Z. and J.P.C. wrote the paper, and all authors edited it. J.P.C. obtained funding for this study.

ACKNOWLEDGMENTS

We thank all members of the J.P.C. lab for useful discussion and experimental help, and special thanks for advice go to our former lab members Jessica Greenwood and Ofer Rog. We thank Alexander Kelly for valuable discussion and Alessandro Bianchi and Miguel Godinho Ferreira for kind gifts of reagents and advice. This work was supported by Cancer Research UK and the National Cancer Institute.

Received: April 4, 2016
Revised: May 6, 2016
Accepted: May 18, 2016
Published: June 16, 2016

REFERENCES

Barefield, C., and Karlseder, J. (2012). The BLM helicase contributes to telomere maintenance through processing of late-replicating intermediate structures. Nucleic Acids Res. *40*, 7358–7367.

Baumann, C., Körner, R., Hofmann, K., and Nigg, E.A. (2007). PICH, a centromere-associated SNF2 family ATPase, is regulated by Plk1 and required for the spindle checkpoint. Cell *128*, 101–114.

Carneiro, T., Khair, L., Reis, C.C., Borges, V., Moser, B.A., Nakamura, T.M., and Ferreira, M.G. (2010). Telomeres avoid end detection by severing the checkpoint signal transduction pathway. Nature *467*, 228–232.

Chan, K.L., and Hickson, I.D. (2011). New insights into the formation and resolution of ultra-fine anaphase bridges. Semin. Cell Dev. Biol. *22*, 906–912.

Chan, K.L., North, P.S., and Hickson, I.D. (2007). BLM is required for faithful chromosome segregation and its localization defines a class of ultrafine anaphase bridges. EMBO J. *26*, 3397–3409.

Chan, K.L., Palmai-Pallag, T., Ying, S., and Hickson, I.D. (2009). Replication stress induces sister-chromatid bridging at fragile site loci in mitosis. Nat. Cell Biol. *11*, 753–760.

Chapman, J.R., Barral, P., Vannier, J.B., Borel, V., Steger, M., Tomas-Loba, A., Sartori, A.A., Adams, I.R., Batista, F.D., and Boulton, S.J. (2013). RIF1 is essential for 53BP1-dependent nonhomologous end joining and suppression of DNA double-strand break resection. Mol. Cell *49*, 858–871.

Cornacchia, D., Dileep, V., Quivy, J.P., Foti, R., Tili, F., Santarella-Mellwig, R., Antony, C., Almouzni, G., Gilbert, D.M., and Buonomo, S.B. (2012). Mouse Rif1 is a key regulator of the replication-timing programme in mammalian cells. EMBO J. *31*, 3678–3690.

Davé, A., Cooley, C., Garg, M., and Bianchi, A. (2014). Protein phosphatase 1 recruitment by Rif1 regulates DNA replication origin firing by counteracting DDK activity. Cell Rep. *7*, 53–61.

Dehé, P.M., Rog, O., Ferreira, M.G., Greenwood, J., and Cooper, J.P. (2012). Taz1 enforces cell-cycle regulation of telomere synthesis. Mol. Cell *46*, 797–808.

Di Virgilio, M., Callen, E., Yamane, A., Zhang, W., Jankovic, M., Gitlin, A.D., Feldhahn, N., Resch, W., Oliveira, T.Y., Chait, B.T., et al. (2013). Rif1 prevents resection of DNA breaks and promotes immunoglobulin class switching. Science *339*, 711–715.

Ding, D.Q., Yamamoto, A., Haraguchi, T., and Hiraoka, Y. (2004). Dynamics of homologous chromosome pairing during meiotic prophase in fission yeast. Dev. Cell *6*, 329–341.

Escribano-Díaz, C., Orthwein, A., Fradet-Turcotte, A., Xing, M., Young, J.T., Tkáč, J., Cook, M.A., Rosebrock, A.P., Munro, M., Canny, M.D., et al. (2013). A cell cycle-dependent regulatory circuit composed of 53BP1-RIF1 and BRCA1-CtIP controls DNA repair pathway choice. Mol. Cell *49*, 872–883.

Germann, S.M., Schramke, V., Pedersen, R.T., Gallina, I., Eckert-Boulet, N., Oestergaard, V.H., and Lisby, M. (2014). TopBP1/Dpb11 binds DNA anaphase bridges to prevent genome instability. J. Cell Biol. *204*, 45–59.

Germe, T., Miller, K., and Cooper, J.P. (2009). A non-canonical function of topoisomerase II in disentangling dysfunctional telomeres. EMBO J. *28*, 2803–2811.

Gregan, J., Polakova, S., Zhang, L., Tolić-Nørrelykke, I.M., and Cimini, D. (2011). Merotelic kinetochore attachment: causes and effects. Trends Cell Biol. *21*, 374–381.

Hardy, C.F., Sussel, L., and Shore, D. (1992). A RAP1-interacting protein involved in transcriptional silencing and telomere length regulation. Genes Dev. *6*, 801–814.

Hayano, M., Kanoh, Y., Matsumoto, S., Renard-Guillet, C., Shirahige, K., and Masai, H. (2012). Rif1 is a global regulator of timing of replication origin firing in fission yeast. Genes Dev. *26*, 137–150.

Hengeveld, R.C., de Boer, H.R., Schoonen, P.M., de Vries, E.G., Lens, S.M., and van Vugt, M.A. (2015). Rif1 is required for resolution of ultrafine DNA bridges in anaphase to ensure genomic stability. Dev. Cell *34*, 466–474.

Hiraga, S., Alvino, G.M., Chang, F., Lian, H.Y., Sridhar, A., Kubota, T., Brewer, B.J., Weinreich, M., Raghuraman, M.K., and Donaldson, A.D. (2014). Rif1 controls DNA replication by directing Protein Phosphatase 1 to reverse Cdc7-mediated phosphorylation of the MCM complex. Genes Dev. *28*, 372–383.

Hofmann, J.F., and Beach, D. (1994). cdt1 is an essential target of the Cdc10/Sct1 transcription factor: requirement for DNA replication and inhibition of mitosis. EMBO J. *13*, 425–434.

Kanoh, J., and Ishikawa, F. (2001). spRap1 and spRif1, recruited to telomeres by Taz1, are essential for telomere function in fission yeast. Curr. Biol. *11*, 1624–1630.

Kanoh, Y., Matsumoto, S., Fukatsu, R., Kakusho, N., Kono, N., Renard-Guillet, C., Masuda, K., Iida, K., Nagasawa, K., Shirahige, K., and Masai, H. (2015). Rif1 binds to G quadruplexes and suppresses replication over long distances. Nat. Struct. Mol. Biol. *22*, 889–897.

Lian, H.Y., Robertson, E.D., Hiraga, S., Alvino, G.M., Collingwood, D., McCune, H.J., Sridhar, A., Brewer, B.J., Raghuraman, M.K., and Donaldson, A.D. (2011). The effect of Ku on telomere replication time is mediated by telomere length but is independent of histone tail acetylation. Mol. Biol. Cell *22*, 1753–1765.

Lukas, C., Savic, V., Bekker-Jensen, S., Doil, C., Neumann, B., Pedersen, R.S., Grøfte, M., Chan, K.L., Hickson, I.D., Bartek, J., and Lukas, J. (2011). 53BP1 nuclear bodies form around DNA lesions generated by mitotic transmission of chromosomes under replication stress. Nat. Cell Biol. *13*, 243–253.

Maciejowski, J., Li, Y., Bosco, N., Campbell, P.J., and de Lange, T. (2015). Chromothripsis and Kataegis Induced by Telomere Crisis. Cell *163*, 1641–1654.

Mattarocci, S., Shyian, M., Lemmens, L., Damay, P., Altintas, D.M., Shi, T., Bartholomew, C.R., Thomä, N.H., Hardy, C.F., and Shore, D. (2014). Rif1 controls DNA replication timing in yeast through the PP1 phosphatase Glc7. Cell Rep. *7*, 62–69.

Miller, K.M., and Cooper, J.P. (2003). The telomere protein Taz1 is required to prevent and repair genomic DNA breaks. Mol. Cell *11*, 303–313.

Miller, K.M., Ferreira, M.G., and Cooper, J.P. (2005). Taz1, Rap1 and Rif1 act both interdependently and independently to maintain telomeres. EMBO J. *24*, 3128–3135.

Miller, K.M., Rog, O., and Cooper, J.P. (2006). Semi-conservative DNA replication through telomeres requires Taz1. Nature *440*, 824–828.

Muñoz, P., Blanco, R., de Carcer, G., Schoeftner, S., Benetti, R., Flores, J.M., Malumbres, M., and Blasco, M.A. (2009). TRF1 controls telomere length and mitotic fidelity in epithelial homeostasis. Mol. Cell. Biol. *29*, 1608–1625.

Nera, B., Huang, H.S., Lai, T., and Xu, L. (2015). Elevated levels of TRF2 induce telomeric ultrafine anaphase bridges and rapid telomere deletions. Nat. Commun. *6*, 10132.

Ohishi, T., Muramatsu, Y., Yoshida, H., and Seimiya, H. (2014). TRF1 ensures the centromeric function of Aurora-B and proper chromosome segregation. Mol. Cell. Biol. *34*, 2464–2478.

Rog, O., Miller, K.M., Ferreira, M.G., and Cooper, J.P. (2009). Sumoylation of RecQ helicase controls the fate of dysfunctional telomeres. Mol. Cell *33*, 559–569.

Sato, M., Dhut, S., and Toda, T. (2005). New drug-resistant cassettes for gene disruption and epitope tagging in Schizosaccharomyces pombe. Yeast *22*, 583–591.

Sfeir, A., Kosiyatrakul, S.T., Hockemeyer, D., MacRae, S.L., Karlseder, J., Schildkraut, C.L., and de Lange, T. (2009). Mammalian telomeres resemble fragile sites and require TRF1 for efficient replication. Cell *138*, 90–103.

Shi, T., Bunker, R.D., Mattarocci, S., Ribeyre, C., Faty, M., Gut, H., Scrima, A., Rass, U., Rubin, S.M., Shore, D., and Thomä, N.H. (2013). Rif1 and Rif2 shape telomere function and architecture through multivalent Rap1 interactions. Cell *153*, 1340–1353.

Silverman, J., Takai, H., Buonomo, S.B., Eisenhaber, F., and de Lange, T. (2004). Human Rif1, ortholog of a yeast telomeric protein, is regulated by

ATM and 53BP1 and functions in the S-phase checkpoint. Genes Dev. *18*, 2108–2119.

Sofueva, S., Osman, F., Lorenz, A., Steinacher, R., Castagnetti, S., Ledesma, J., and Whitby, M.C. (2011). Ultrafine anaphase bridges, broken DNA and illegitimate recombination induced by a replication fork barrier. Nucleic Acids Res. *39*, 6568–6584.

Sreesankar, E., Senthilkumar, R., Bharathi, V., Mishra, R.K., and Mishra, K. (2012). Functional diversification of yeast telomere associated protein, Rif1, in higher eukaryotes. BMC Genomics *13*, 255.

Xu, L., and Blackburn, E.H. (2004). Human Rif1 protein binds aberrant telomeres and aligns along anaphase midzone microtubules. J. Cell Biol. *167*, 819–830.

Xu, D., Muniandy, P., Leo, E., Yin, J., Thangavel, S., Shen, X., Ii, M., Agama, K., Guo, R., Fox, D., 3rd., et al. (2010). Rif1 provides a new DNA-binding interface for the Bloom syndrome complex to maintain normal replication. EMBO J. *29*, 3140–3155.

Xue, Y., Rushton, M.D., and Maringele, L. (2011). A novel checkpoint and RPA inhibitory pathway regulated by Rif1. PLoS Genet. *7*, e1002417.

Yamazaki, S., Hayano, M., and Masai, H. (2013). Replication timing regulation of eukaryotic replicons: Rif1 as a global regulator of replication timing. Trends Genet. *29*, 449–460.

Zimmermann, M., Lottersberger, F., Buonomo, S.B., Sfeir, A., and de Lange, T. (2013). 53BP1 regulates DSB repair using Rif1 to control 5′ end resection. Science *339*, 700–704.

Cell Reports, Volume *16*

Supplemental Information

Rif1 Regulates the Fate of DNA Entanglements during Mitosis

Sophie Zaaijer, Nadeem Shaikh, Rishi Kumar Nageshan, and Julia Promisel Cooper

Figure S1

A

taz1Δ - 19°C - **Tpz1 Histone H3**

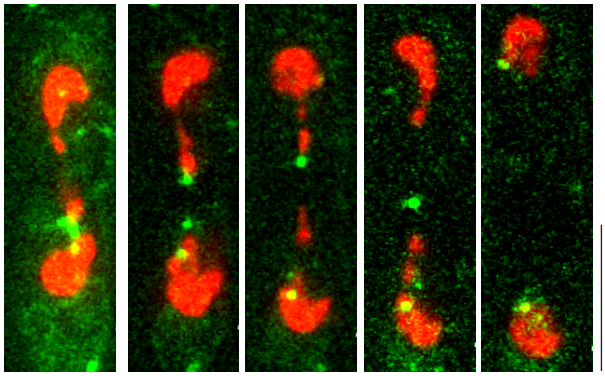

B

Polα persistence in G2 cells

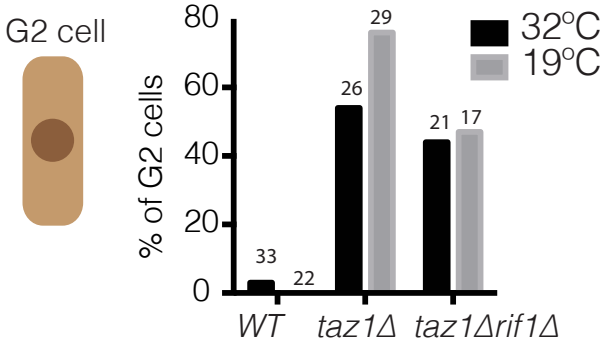

taz1Δ 19°C

Polα **Histone H3**

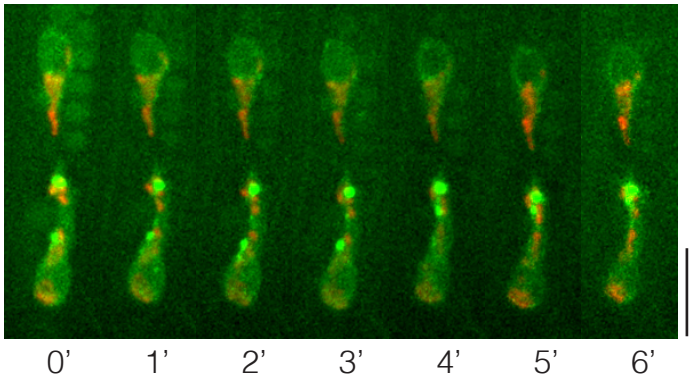

C

taz1Δ - 19°C **Rad52 Histone H3**

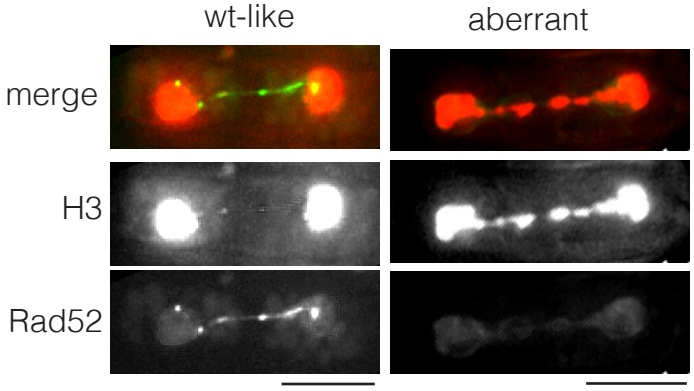

Rad52 presence in the midzone in *taz1Δ* cells

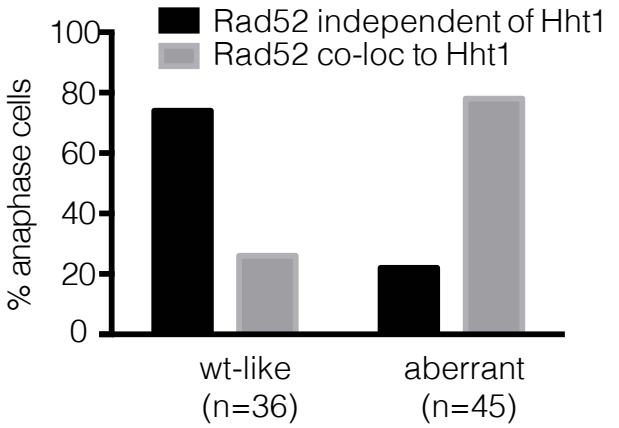

Figure S1, related to Figure 3: DNA replication and repair proteins appear in the anaphase mid-region in a *taz1Δ* setting.

A) Stills from a representative film of *taz1Δ* cells harboring endogenously tagged Tpz1-GFP and histone H3 as in Figure 1. Images were captured every 2 minutes through anaphase.

B) Cells harboring endogenously tagged Polα-GFP and histone H3 were grown to log phase at 32°C, then shifted to 19°C for 24 hours. Left panel: percentage of G2 cells showing Polα -GFP foci. Right panel: frames from film of a *taz1Δ* cell completing anaphase. Numbers below panels indicate time since filming began.

C) *taz1Δ* cells tagged at endogenous loci for Rad52 and histone H3 were followed through anaphase and categorized as showing either wt-like or aberrant chromosome segregation. Left: representative images. Right: Quantitation of presence of Rad52 between segregating chromosomes.

Figure S2

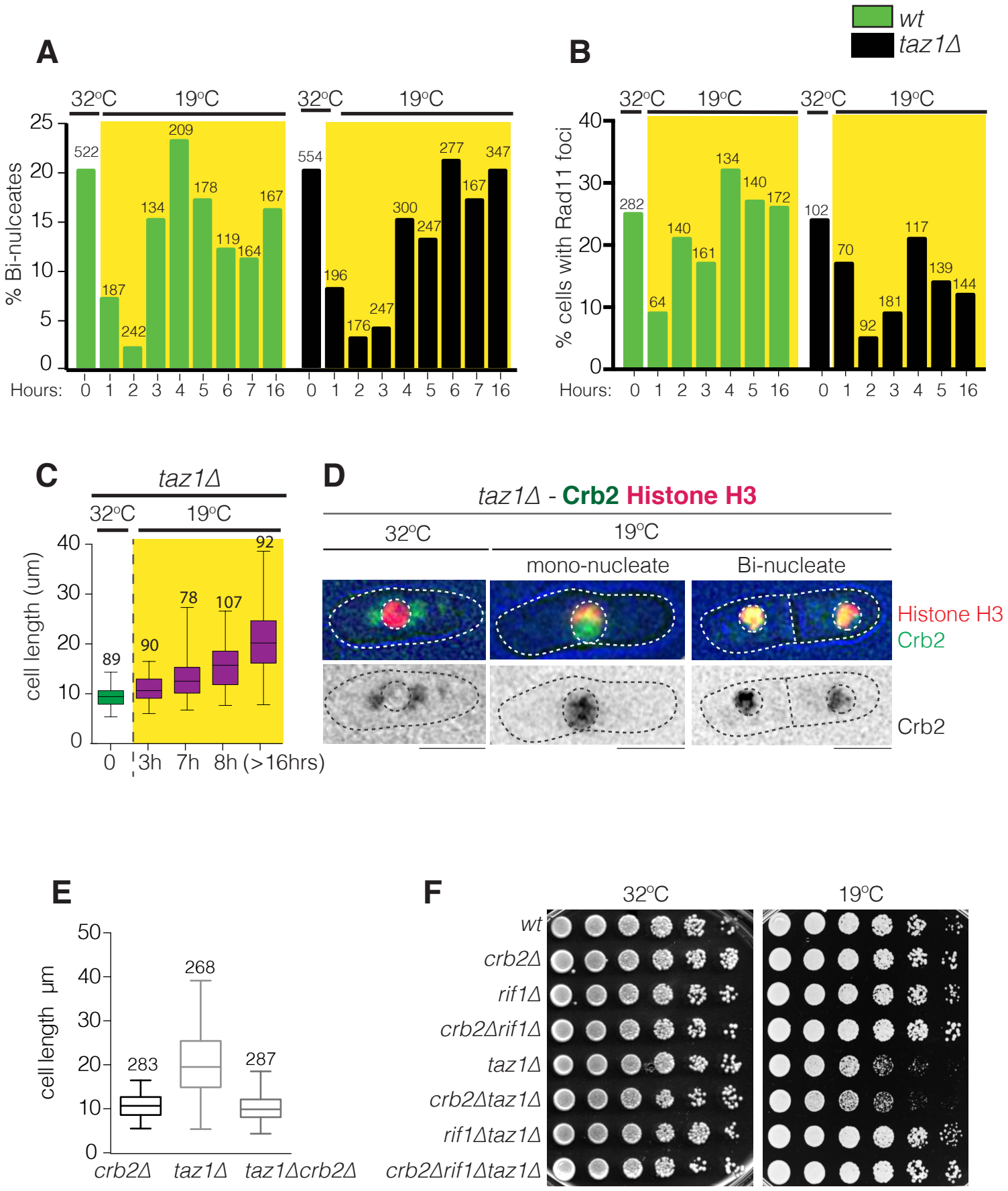
A
B
wt
taz1Δ
32°C
19°C
% Bi-nucleates
% cells with Rad11 foci
Hours:
C
taz1Δ
cell length (um)
0
3h
7h
8h (>16hrs)
D
taz1Δ - Crb2 Histone H3
mono-nucleate
Bi-nucleate
Histone H3
Crb2
E
cell length µm
crb2Δ
taz1Δ
taz1Δcrb2Δ
F
wt
crb2Δ
rif1Δ
crb2Δrif1Δ
taz1Δ
crb2Δtaz1Δ
rif1Δtaz1Δ
crb2Δrif1Δtaz1Δ

Figure S2, related to Figure 4: *taz1Δ* cells trigger the Crb2^{53BP1}-dependent checkpoint only in the second cell cycle following shift to cold temperature.

A) Bi-nucleate status (indicative of G1/S phase) is monitored in *wt* and *taz1Δ* cultures. Numbers below the x-axis indicate hours after shift from 32°C to 19°C. See text for details.
B) The presence of Rad11^{RPA}-GFP foci (indicative of S phase) is monitored as in (A).

C) *taz1Δ* cell length over time in the cold. Cells were grown to log phase at 32°C, then shifted to 19°C. X-axis labels indicate hours after the temperature shift.

D) Crb2^{53BP1} localization is viewed in log phase at 32°C and >8 hours after shift to 19°C.

E) Cells grown to log-phase at 32°C were shifted to 19°C for 24 hours; then, cell lengths were measured.

F) Five-fold serial dilutions of log-phase cultures grown at 32°C were spotted onto rich medium and incubated at 32°C for 2 days or 19°C for 5 days.

Figure S3

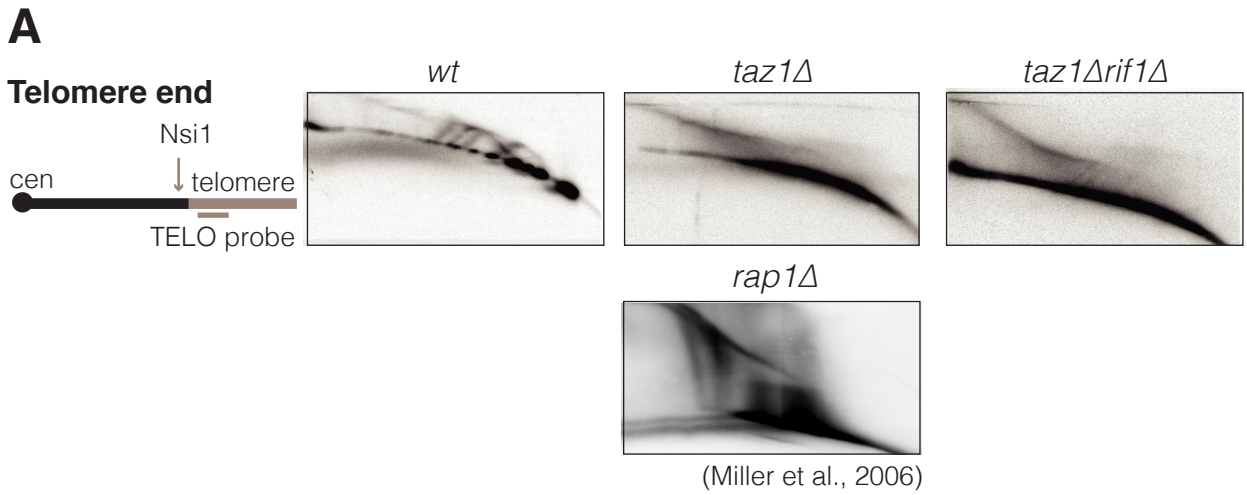
A
Telomere end
Nsi1
cen
telomere
TELO probe
wt
taz1Δ
taz1Δrif1Δ
rap1Δ
(Miller et al., 2006)

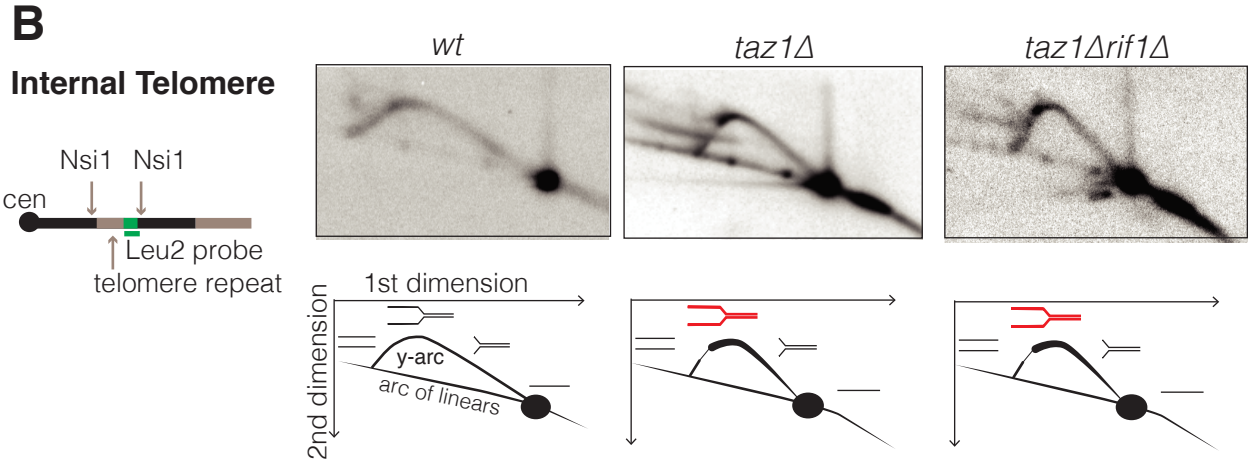
B
Internal Telomere
Nsi1
Nsi1
cen
Leu2 probe
telomere repeat
wt
taz1Δ
taz1Δrif1Δ
1st dimension
2nd dimension
y-arc
arc of linears

Figure S3, related to Figure 4: Rif1 neither causes nor suppresses *taz1Δ* telomere replication defects.
(A and B) Left: Diagrams indicating positions of NsiI restriction sites and probes. The internal telomere was constructed by inserting a cassette containing a synthetic telomere repeat tract and the *ScLEU2* gene at the *ura4+* locus on Chr III (Miller et al., 2006). Right: Southern blots of two-dimensional gels of NsiI fragments, hybridized with the telomere probe (A) or the Leu2 probe (B). Below each blot is an interpretive diagram.

A) While Y-arcs indicative of complete replication are seen for telomeric DNA isolated from *wt* cells, the corresponding arcs for *taz1Δ* telomeres fail to return to the arc of linears, indicating stalled, incomplete replication. *rap1Δ* telomeres are shown for comparison; while *rap1Δ* telomeres are long and heterogeneous, the corresponding Y-arcs both ascend and descend back to the arc of linears (*rap1Δ* image is re-printed from (Miller et al., 2006)).

B) The internal telomere was specifically assessed by hybridizing with a probe for *ScLEU2*. Prominent fork stalling is seen at this region in *taz1Δ* and *taz1Δrif1Δ* cells alike.

Figure S4

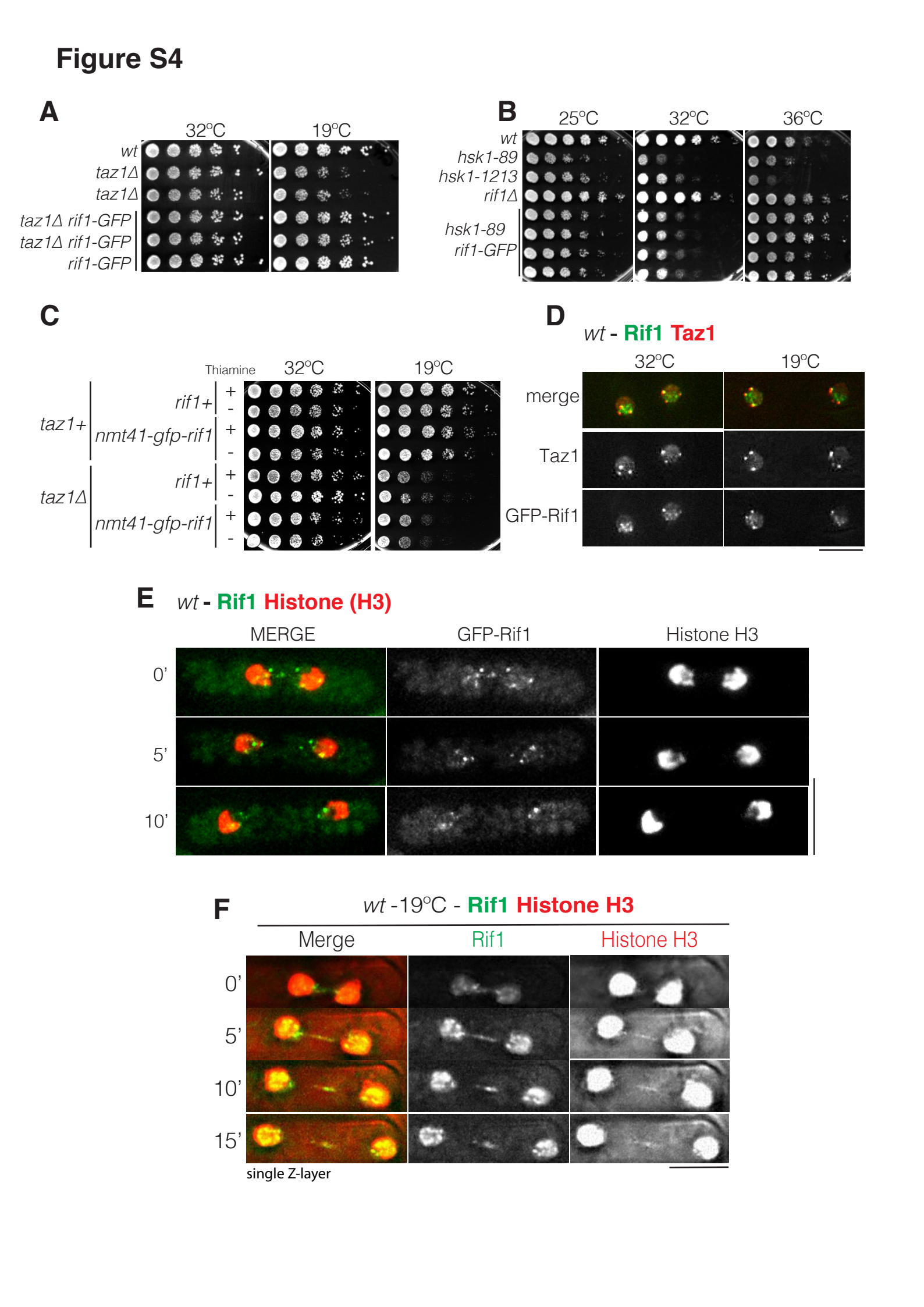
A
32°C
19°C
wt
taz1Δ
taz1Δ
taz1Δ rif1-GFP
taz1Δ rif1-GFP
rif1-GFP
B
25°C
32°C
36°C
wt
hsk1-89
hsk1-1213
rif1Δ
hsk1-89
rif1-GFP
C
Thiamine
32°C
19°C
taz1+
rif1+
nmt41-gfp-rif1
taz1Δ
rif1+
nmt41-gfp-rif1
D
wt - Rif1 Taz1
32°C
19°C
merge
Taz1
GFP-Rif1
E
wt - Rif1 Histone (H3)
MERGE
GFP-Rif1
Histone H3
0'
5'
10'
F
wt -19°C - Rif1 Histone H3
Merge
Rif1
Histone H3
0'
5'
10'
15'
single Z-layer

Figure S4, related to Figure 5: Behavior of N- and C-terminally GFP tagged Rif1.

A) Five-fold serial dilutions of log-phase cultures were spotted onto rich medium and incubated at 32°C for 2 days or 19°C for 5 days.

B) Serial dilutions were plated as in (A) and grown at 25°C for 5 days, or 32°C or 36°C for 2 days

C) Cells were maintained in log phase in minimal liquid media with or without 60 μM thiamine (the absence of which confers induction of expression from the *nmt41* promoter) for 3 days at 32°C. Five-fold serial dilutions were then spotted onto rich media and incubated at 32°C for 2 days or 19°C for 5 days.

D) Representative images of G2-phase cells harboring endogenously tagged Taz1-mCherry and GFP-Rif1. Cells were grown to log phase at 32°C, then shifted to 19°C for 24 hours.

E) Frames from representative film of a cell as it progresses from G2 to anaphase at 32°C. No GFP-Rif1 is detected in the mid-region between segregating chromosomes. Compare with Figure 5A.

F) Frames from a representative film of a cell grown to log phase at 32°C, then shifted to 19°C for 24 hours. In contrast to all other microscopy images in which multiple stacks in Z-axis were collapsed into one, these images represent a single plane in the Z-axis.

Figure S5

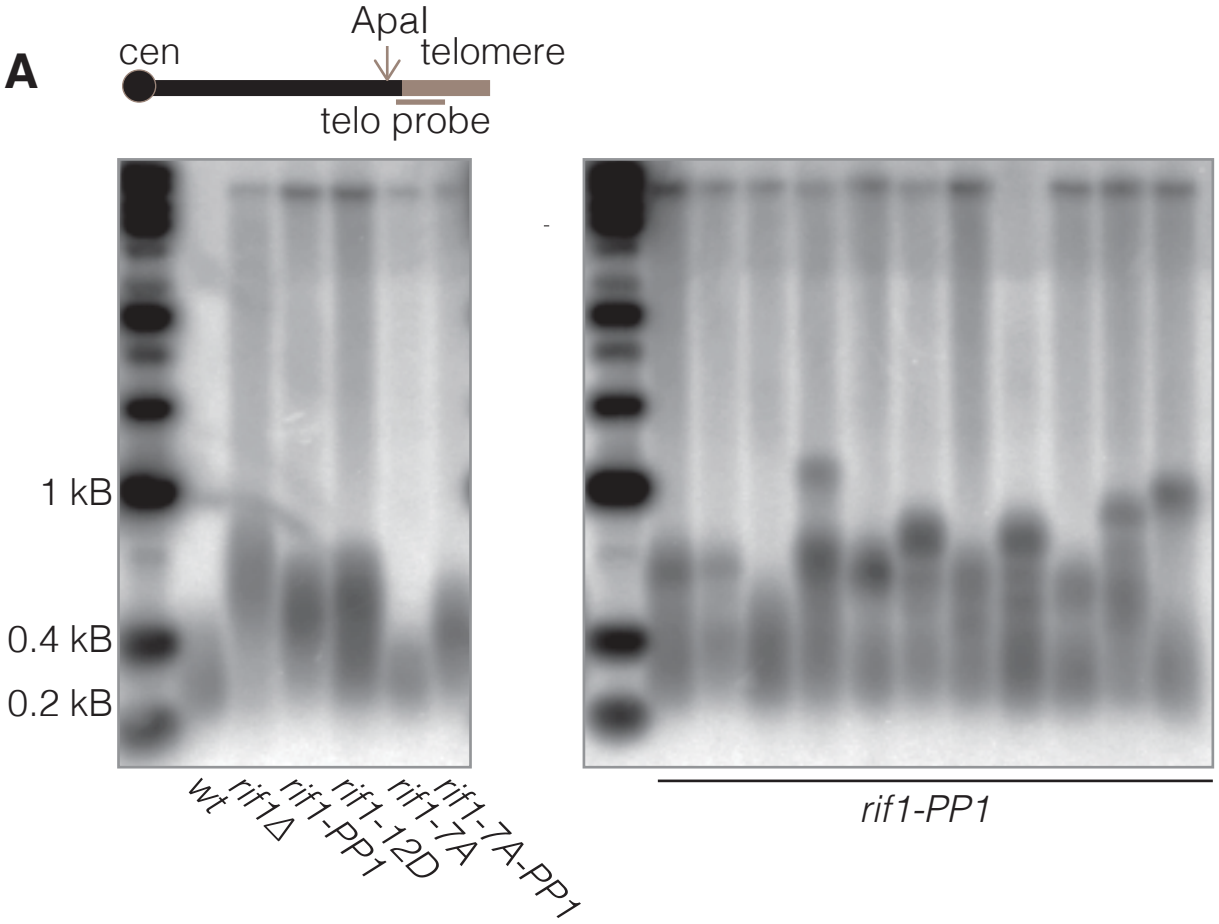
A
cen
ApaI
telomere
telo probe
1 kB
0.4 kB
0.2 kB
wt
rif1Δ
rif1-PP1
rif1-12D
rif1-7A
rif1-7A-PP1
rif1-PP1

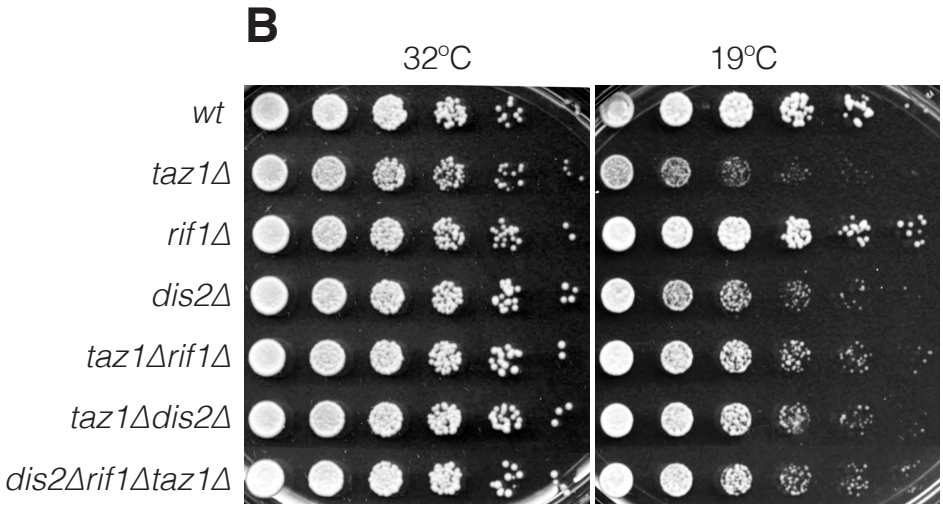
B
32°C
19°C
wt
taz1Δ
rif1Δ
dis2Δ
taz1Δrif1Δ
taz1Δdis2Δ
dis2Δrif1Δtaz1Δ

Figure S5, related to Figure 6: The loss of Rif1's PP1-binding ability, or the loss of PP1 phosphatase, rescues *taz1Δ* cold sensitivity.

A) Telomere lengths were analyzed by Southern blot analysis of Apa1 digested genomic DNA, hybridized with a telomere probe. The multiple *rif1-pp1* single clones in the right panel were constructed by crossing a *rif1Δ* strain against a *rif1-pp1* strain (Dave et al., 2014).

B) Five-fold serial dilutions of log-phase cultures were spotted onto rich medium and incubated at 32°C for 2 days or 19°C for 5 days. Dis2 is one of the two fission yeast PP1 phosphatases; see text for details.

Supplemental Movie Legends:

Movie S1: Film (stills in Figure 1A), showing a *taz1Δ* cell, harboring fluorescent histone H3 (see Figure 1A) and grown at 19˚C, with a "*wt*-like" chromosome segregation pattern.

Movie S2: Film of a *taz1Δ* cell tagged as in Figure 1A exhibiting the "pointing finger" segregation phenotype (see Figure 1A and text).

Movie S3: Film of a *taz1Δ* cell tagged as in Figure 1A demonstrating the "irreversibly entangled" segregation pattern (see Figure 1A and text).

Movie S4: Film (stills in Figure 3E) of *taz1Δ* cell carrying mRFP-tagged histone H3 and GFP-tagged RPA^{Rad11}. This cell, grown at 19˚C, shows a strand of RPA between segregating chromosomes retracting into one of the daughter nuclei.

Table S1. Strains constructed and analysed in this study

JCF N°	Mating type	*Genotype*	Origin
11	h^+	*taz1::ura4$^+$ ade6-M216 leu1-32 ura4-D18*	Lab Stock
108	h^-	*ade6-M210 his3-D1 leu1-32 ura4-D18*	Lab Stock
109	h^+	*ade6-M216 his3-D1 leu1-32 ura4-D18*	Lab Stock
282	h^-	*rif1::kanMX6 taz1::ura4$^+$ ade6-(M210 or M216) leu1-32 ura4-D18*	Lab Stock
300	h^-	*rif1::kanMX6 ade6-M216*	Lab stock
481	h^-	*rif1-GFP:kanMX6*	Lab Stock
1076	h^+/h^-	*trt1$^+$/trt1::hygMX6 ade6-M210/ade6-M216 his3-D1/his3-D1 leu1-32/leu1-32 ura4-D18/ura4-D18*	Lab Stock
1582	h^+/h^-	*taz1::kanMX6/taz1::kanMX6 trt1$^+$/trt1::his3 ade6-M210/ade6-M216 his3-D1/his3-D1 leu1-32/leu1-32 ura4-D18/ura4-D18*	Lab Stock
1675	h^+	*ura4::synthetic-telo (500bp) his3- leu1-32 ade6-(M210 or M216)*	Lab stock
1678	h^+	*ura4::synthetic-telo (500bp) taz1::kanMX6 his3- leu1-32 ade6-(M210 or M216)*	Lab stock
1689	*h?*	*ura4::synthetic-telo (500bp) rif1::kanMX6 taz1::hygMX6 his3- leu1-32 ade6-(M210 or M216)*	Lab stock
2906	h^-	*lys1:kanMX6:nmt1:GFP-atb2 leu1-32 ura4-D18*	Nurse Lab (PN3774)
4496	h^-	*hht1-mRFP:kanMX6 ade6-M210 leu1-32 ura4-D18 his3-D1*	Lab stock
6382	h^-	*hsk1-1312 ade6-M216 leu1-32 ura4-D18*	Forsburg lab
9202	h^-	*crb2::ura4$^+$ ade6-M216 his3-D1 leu1-32 ura4-D18*	This study
9203	h^+	*rif1::hygMX6 his3-D1 leu1-32 ura4-D18*	This study
9204	h^+	*crb2::ura4$^+$ rif1::hygMX6 ade6-M216 his3-D1 leu1-32 ura4-D18*	This study
9205	h^-	*taz1::natMX6 his3-D1 leu1-32 ura4-D18*	This study
9206	h^+	*taz1::natMX6 crb2::ura4$^+$ ade6-M216 his3-D1 leu1-32 ura4-D18*	This study
9207	*h?*	*taz1::natMX6 rif1::hygMX6 ade6-M216 his3-D1 leu1-32 ura4-D18*	This study
9208	h^+	*taz1::natMX6 rif1::hygMX6 crb2::ura4$^+$ his3-D1 leu1-32 ura4-D18*	This study
9236	h^+/h^-	*taz1::kanMX6/taz1::kanMX6 rif1+/rif1::hygMX6 trt1$^+$/trt1::his3$^+$ ade6-M201/ade6-M216 his3-D1/his3-D1 leu1-32/leu1-32 ura4-D18/ura4-D18*	This study
9273	h^-	*rif1-GFP:kanMX6 taz1::hygMX6*	This study
9292	$h^?$	*hht1-mRFP:kanMX6 reb1-GFP:natMX6 taz1::hygMX6 leu1-32 ura4-D18 his3-D1*	This study
9298	h^-	*hht1-mRFP:kanMX6 taz1::hygMX6 ade6-M210 leu1-32 ura4-D18 his3-D1*	This study
9301	$h^?$	*hht1-mRFP:kanMX6 taz1-GFP:kanMX6 ade6-(M210 or M216) leu1-32 ura4-D18 his3-D1*	This study
9306	h^-	*hht1-mRFP:kanMX6 taz1::hyg rif1::natMX6 ade6-M210 leu1-32 ura4-D18 his3-D1*	This study
9317	h^-	*kanMX6:nmt41:GFP-rif1 ade6-M210 his3-D1 leu1-32 ura4-D18*	This study
9319	$h^?$	*kanMX6:nmt41:GFP-rif1 taz1::natMX6 ade6-M210 his3-D1 leu1-32 ura4-D18*	This study
9328	*h?*	*rif1-GFP:kanMX6 hsk1-89:ura4$^+$*	This study
9339	$h^?$	*kanMX6:nmt41:GFP-rif1 taz1-mCherry:natMX6 ade6-(M210 or M216) his3-D1 leu1-32 ura4-D18*	This study
9363	$h^?$	*ade6-216 leu1-32 lys1-131 ura4-D18 sod2[::kanMX6-ura4+-lacOp] his7+::lacI-GFP hht1-mRFP:kanMX6 taz1::natMX6*	This study
9375	h^+	*tpz1-GFP:kanMX6 hht1-mRFP:kanMX6 taz1::natMX6 his3-D1 leu1-32 ura4-D18*	This study
9378	$h^?$	*hht1-mRFP:kanMX6 rad11-GFP:kanMX6 taz1::hygMX6 ade6-M210 his3-D1 leu1-32 ura4-D18*	This study

Table S1. Strains constructed and analysed in this study

10368	h^{90}	*z:NatR-P-adh131-tetR-tomato cnt2::TetO::ura4+*	Lab stock
11330	h^-	*hht1-mRFP:kanMX6 rad22-GFP:kanMX6 taz1::ura4+ ade6-M210 his3-D1 leu1-32 ura4-D18*	This study
11337	h^+	*crb2-D2::ura4+ leu1-32::2xYFP-crb2:leu1+ ura4-D18 taz1::kanMX6 hht1-mRFP:kanMX6*	This study
11357	$h^?$	*hht1-mRFP:kanMX6 kanMX6:nmt41-GFP-rif1 ade6-M216 his3-D1 leu1-32 ura4-D18*	This study
11382	h^-	*swi7-GFP:kanMX6 hht1-mRFP:kanMX6 his3-D1*	This study
11384	h^+	*swi7-GFP:kanMX6 hht1-mRFP:kanMX6 taz1::hygMX6 his3-D1 leu1-32*	This study
11394	h^-	*swi7-GFP:kanMX6 hht1-mRFP:kanMX6 taz1::hygMX6 rif1::natMX6 his3-D1*	This study
11429	$h^?$	*hht1-mRFP:kanMX6 kanMX6:nmt41-GFP-rif1 taz1::natMX6 ade6-(M210 or M216)*	This study
11475	$h^?$	*hht1-mRfP:kanMX6 rad11-GFP:kanMX6 taz1::hyg rif1::natMX6 ade6-(M210 his3-D1 leu1-32 ura4-D18*	This study
12320	h^+	*rif1-PP1 ade6-216 his3-D1 ura4-D18 leu1-32*	Bianchi lab
12322	h^-	*rif1-12D ade6-216 his3-D1 ura4-D18 leu1-32*	Bianchi lab
12323	h^+	*rif1-7a ade6-216 his3-D1 ura4-D18 leu1-32*	Bianchi lab
12324	h^-	*rif1-7a-PP1 ade6-216 his3-D1 ura4-D18 leu1-32*	Bianchi lab
12333	h^-	*taz1::kanMX6 rif1-PP1 his3-D1*	This study
12361	$h^?$	*hht1-mRFP:kanMX6 rad11-GFP:kanMX6 ade6-M210 ura4-D18*	This study
12372	$h^?$	*rif1-PP1 z:NatR-Padh131-TetR-tomato cnt2::TetO*2::ura4 ura4-D18*	This study
12373	h^{90}	*rif1::hygMX6 z:NatR-Padh131-TetR-tomato cnt2::TetO*2::ura4 ura4-D18*	This study
12374	$h^?$	*rif1::hygMX6 z:NatR-Padh131-TetR-tomato cnt2::TetO*2::ura4 ura4-D18*	This study
12392	$h^?$	*z:NatR-Padh131-TetR-tomato*	This study
13431	h^+	*rif1::bsd hsk1-89:ura4+ ura4-D18 leu1-32*	Bianchi lab
13433	h^-	*hsk1-89:ura4+ ura4-D18 leu1-32*	Bianchi lab
13524	*h?*	*hht1-mRFP:kanMX6 reb1-GFP:natMX6 leu1-32 ura4-D18 his3-D1*	This study
13546	h^-	*pcdt1-rif1 ura4-D18 leu1-32 ade6-M210 his3-D1*	This study
13547	h^-	*pcdt1-rif1 ura4-D18 leu1-32 ade6-M210 his3-D1*	This study
13579	*h?*	*taz1::ura4+ pcdt1-rif1 ade6-(M210 or M216) leu1-32 ura4-D18*	This study
13616	h^+	*taz1::ura4+ pcdt1-rif1 ade6-M216 leu1-32 ura4-D18*	This study
13632	h^-	*hsk1-89:ura4+ pcdt1-rif1 ura4-D18 leu1-32*	This study
13670	$h^?$	*pcdt1-rif1 z:NatR-Padh131-TetR-tomato cnt2::TetO*2::ura4 ura4-D18*	This study
13829	h^-	*rif1::hygMX6 ade6-M210 his3-D1 ura4-D18 leu1-32*	This study
13831	h^+	*dis2::ura4+ ura4-D18 leu1-32 ade6-M216 his3-D1*	This study
13835	$h^?$	*taz1::natMX6 rif1::hygMX6 ade6-M216 his3-D1 ura4-D18 leu1-32*	This study
13837	h^-	*dis2::ura4+ taz1::natMX6 ura4-D18 leu1-32*	This study
13840	h^-	*dis2::ura4+ rif1::hygMX6 ade6-M216 his3-D1 ura4-D18 leu1-32*	This study
13843	h^-	*dis2::ura4+ rif1::hygMX6 taz1::natMX6 ade6-M216 his3-D1 ura4-D18 leu1-32*	This study
13846	$h^?$	*taz1::natMX6 ade6-M216 his3-D1 ura4-D18 leu1-32*	This study

Supplemental Experimental Procedures

Strains and media

Media and growth conditions were as previously described (Moreno et al., 1991). Strains are listed in Table S1. Single gene deletions and tag insertions were generated as described (Bahler et al., 1998) and used to create further strains through crossing and sporulation. The *taz1Δ rif1-pp1* clones were generated by crossing a *taz1Δrif1Δ* strain to a *rif1-pp1* strain; single *taz1Δ rif1-PP1* clones were selected.

Molecular Biology Techniques

Southern blot and two-dimensional gel electrophoresis were performed as previously described (Miller et al., 2006) using described probes (Rog et al., 2009).

qRT PCR:

RNA was harvested from cultures using MasterPure Yeast RNA Purification kit as described in the manufacturer's protocol (Epicentre). cDNA was generated using 2μg RNA, oligo dT primers and Superscript III Reverse Transcriptase kit (ThermoFisher). Transcripts were quantified using EXPRESS SYBR GreenER (ThermoFisher) and the StepOnePlus Real-Time PCR System (ThermoFisher). Primer specificity was confirmed by both melting-curve analysis and agarose gel electrophoresis of PCR products. Transcript levels for *rif1+* were analyzed by the standard curve method and normalized to *act1+* transcript levels.

Live Cell Microscopy

Cells were adhered to 35-mm glass culture dishes (MatTek Corporation) using 0.2 mg/ml of soybean lectin (Sigma-Aldrich) and immersed in YES, or alternatively places on solid media pads (2% agarose melted in YES) on glass slides, with a coverslip sealed on top.

Time-lapse imaging was performed at 27°C in an Environmental Chamber with a DeltaVision Spectris (Applied Precision) comprising a widefield inverted epifluorescence microscope (IX70; Olympus), a 100x NA 1.4 oil immersion objective (UPlanSapo; Olympus), and a charge coupled device CoolSnap HQ camera (Photometrics). Images were acquired over 20 focal planes at a 0.2µm step size with frames taken at different time points. Images were deconvolved (conserved ratio method) and combined into a 2D image using the maximum intensity projection setting for analysis using SoftWorx (Applied Precision). Structural Illumination microscopy was carried out using a DeltaVision OMX (Applied Precision) comprising an OMX optical microscope (version 4), an Olympus PLAPON60xO, NA 1.42, oil immersion objective, and a sCMOS camera.

Supplemental References

Bahler, J., Wu, J.Q., Longtine, M.S., Shah, N.G., McKenzie, A., 3rd, Steever, A.B., Wach, A., Philippsen, P., and Pringle, J.R. (1998). Heterologous modules for efficient and versatile PCR-based gene targeting in Schizosaccharomyces pombe. Yeast *14*, 943-951.

Moreno, S., Klar, A., and Nurse, P. (1991). Molecular genetic analysis of fission yeast Schizosaccharomyces pombe. Methods Enzymol *194*, 795-823.